



UNIVERSITY „POLITEHNICA” OF BUCHAREST
Doctoral School of Industrial Engineering and Robotics

PhD DISSERTATION

-summary-

*Cercetări privind fabricația aditivă prin depunere de filament topit
din polimeri cu temperaturi înalte de procesare*

*Research on additive manufacturing by deposition of molten
filament from polymers with high processing temperatures*

Author, Eng. Aurelian ZAPCIU

Scientific Coordinator, Prof. Eng., PhD George CONSTANTIN

București, 2021

TABLE OF CONTENTS

ABBREVIATIONS.....	6
CH. 1 ADDITIVE MANUFACTURING (AM)	
1.1 HISTORY	
1.2 AM CLASSIFICATION AND PROCESS TYPES	
1.2.1 Stereolithography	
1.2.2 Liquid jet processes	
1.2.3 AM technologies with resin using direct light processing (DLP)	
1.2.4 Selective sintering with laser for polymers (SLS)	
1.2.5 Selective sintering with laser for ceramics and metals	
1.2.6 Direct laser sintering of metals (DMLS)	
1.3 AM APPLICATIONS	
1.4 CURRENT TRENDS	
CH. 2 FDM/FFF TECHNOLOGY – FUSED DEPOSITION MODELING / FUSED FILAMENT FABRICATION	7
2.1 HISTORY OF FDM/FFF	7
2.2 FUNDAMENTAL PRINCIPLES OF THE EXTRUSION PROCESS	8
2.2.1 Material loading	
2.2.2 Material liquifaction (melting)	8
2.2.3 Material extrusion	8
2.2.4 Material solidification.....	10
2.2.5 Position control	
2.2.6 Layer adhesion	10
2.2.7 Generation of support structures	
2.2.8 Control of extruder pathing	
2.3 THE DEMOCRATIZATION OF ADDITIVE MANUFACTURING	
2.4 MATERIALS COMMONLY USED IN FDM/FFF PROCESSES	
2.4.1 Acrylonitrile-butadiene-styrene (ABS)	
2.4.2 Polylactic acid (PLA)	
2.4.3 High impact polystyrene (HIPS)	
2.4.4 Nylon	
2.4.5 Composite materials and wood-plastic composites (WPC)	
2.4.6 Conductive materials	
2.5 RESEARCH AREAS	11
2.5.1 Optimization of volume generation processes for parts manufactured by FDM / FFF processes in order to save material	

2.5.2 Development of support volume generation processes for parts manufactured by FDM / FFF processes	
2.5.3 Development of processes for topological optimization in the context of part manufacturing by additive manufacturing processes.	
2.5.4 Development of processes for additive manufacturing with thermoplastic materials with high processing temperatures.....	11
CH. 3 HARDWARE MODELS OF FFF 3D PRINTERS	13
3.1 CARTESIAN SYSTEMS	
3.1.1 Mechanical and electronic components	
3.1.2 Motion axes drive elements	
3.2 “DELTA” SYSTEMS	
3.2.1 Delta machine platform	
3.2.2 Tool trajectory generation for delta systems	
3.3 PRINTER BED (PRINTING SURFACE)	
3.4 EXTRUDER	
3.4.1 Feedstock feeding system	
3.4.2 Temperature management system	
3.4.3 Extrusion nozzle	
3.4.4 Feedstock	
CH. 4 ELECTRONIC COMPONENTS AND SOFTWARE	
4.1 HUMAN – MACHINE INTERFACE (HMI)	
4.2 SOFTWARE	
4.3 STL FORMAT	
4.4 AMF FORMAT	
4.5 SLICER	
CH. 5 PROCESS PARAMETERS.....	14
5.1 PROCESS PARAMETERS	14
5.2 ENVIRONMENT PARAMETERS	
5.3 DYNAMIC PARAMTERS	
5.3.1 Extrusion speed	
5.3.2 Acceleration	
5.3.3 Position and orientation of printed part	
5.3.4 Extrusion nozzle diameter	
5.3.5 Layer height	
5.3.6 Deposited filament width	
5.3.7 Retraction	
5.3.8 Number of exterior contours	

5.3.9	Number of top and bottom layers	
5.3.10	Part infill and infill pattern	
5.3.11	Filament diameter	
CH. 6	DETERMINING MATERIALS FOR THE CONSTRUCTION OF AN EXTRUDER FOR POLYMERS WITH HIGH PROCESSING TEMPERATURES USING THERMAL FINITE ELEMENT ANALYSIS.....	15
6.1	FINITE ELEMENT ANALYSIS SETUP.....	15
6.2	RESULTS OF THE FINITE ELEMENT ANALYSIS	17
6.3	EXPERIMENTAL DETERMINATION OF THE OPERATING TEMPERATURES OF AN EXTRUDER FOR ADDITIVE MANUFACTURING BY FUSED FILAMENT FABRICATION.....	21
6.4	THERMAL FINITE ELEMENT ANALYSIS OF A PART MANUFACTURED BY FUSED FILAMENT FABRICATION.....	26
6.5	EXPERIMENTAL MEASUREMENT OF INTERIOR TEMPERATURE OF PARTS MADE BY FUSED FILAMENT FABRICATION	32
CH. 7	FDM 3D PRINTER WITH A VACUUM BUILD CHAMBER	38
7.1.	ASPECTS RELATED TO THE BEHAVIOR OF MATERIALS IN A VACUUM	
7.1.1	Losses suffered by anorganic materials	
7.1.2	Losses suffered by organic materials	
7.1.3	Changes in the properties of anorganic materials	
7.1.6	Plastic materials	
7.2.	THERMAL TRANSFER IN A VACUUM	38
7.2.1	Heat transfer in the case of the extruder of a machine for additive manufacturing by fused filament fabrication.....	38
7.2.2	Heat transfer in the case of deposited material	39
7.3	VACUUM BUILD CHAMBER 3D PRINTER DESIGN	40
7.3.1	Dimensioning the resistance structure for the sealed chamber	40
7.3.2	Producing the relative motion of the extruder in relation to the machine platform	41
7.3.3	Linear axes actuation.....	42
7.3.4	Thermoplastic filament extruder	43
7.3.5	Passing electric current through the vacuum chamber walls	44
7.4	WORKING PRINCIPLE.....	45
7.5	MECHANICAL STRUCTURE.....	45
7.6	ELECTRICAL AND ELECTRONIC COMPONENTS	47
7.7	SOFTWARE AND FIRMWARE	48
7.7.1	Firmware	48
7.7.2	Slicer	48
7.7	USER INTERFACE	
CH. 8.	EXPERIMENTAL TESTING AND RESULTS.....	49

8.1 METHOD AND MATERIALS	49
8.2 SURFACE QUALITY AND DIMENSIONAL ACCURACY	49
8.3 TENSILE STRENGTH TESTING	51
8.4 THERMAL BEHAVIOR OF 3D PRINTED PARTS FROM ULTEM 1010.....	53
CH. 9 GENERAL CONCLUSIONS, ORIGINAL CONTRIBUTIONS AND FUTURE RESEARCH DIRECTIONS ...	54
9.1 GENERAL CONCLUSIONS	54
9.2 ORIGINAL CONTRIBUTIONS.....	56
9.3 FUTURE RESEARCH.....	57
BIBLIOGRAPHY.....	58

ABBREVIATIONS

ABS – Acrylonitrile-Butadiene-Styrene polymer;
 AM – Additive manufacturing;
 DLP – Direct Light Processing – a light scanning process;
 DMLS –Direct Metal Laser Sintering – a 3D printing process for printing with metallic powder;
 FDM – Fused Deposition Modeling – a 3D printing process, trademarked;
 FFF – Fused Filament Fabrication) – a 3D printing process, non-trademarked;
 PEI – Polyetherimide polymer;
 PLA – PolyLactic Acid polymer;
 SLS – Selective Laser Sintering – a 3D printing process for printing with polymer powder or polymer-coated metallic powder.

CH. 2 FDM/FFF TECHNOLOGY – FUSED DEPOSITION MODELING – FUSED FILAMENT FABRICATION

2.1 HISTORY OF FDM/FFF

The FDM process was first marketed by Stratasys in 1991, with patents being granted to the company's founder, Scott Crump in 1992 [33]. The machines sold by Stratasys were well received, as the manufacturing process and mechanical structure of the machines were simple compared to those of machines using stereolithography, but the explosion in popularity of the FDM process came with the expiration of the patents held in the field..

The process produces parts by extruding a material, usually a thermoplastic polymer (Fig. 2.1). The extruder pushes a filament of thermoplastic material through a heated nozzle moving in the XY plane to create a two-dimensional layer. This layer is a section of the digital model of the solid that will be 3D-printed. To ensure proper fusion between the layers of material, the base on which the first layer is deposited, or the machine enclosure, is heated.

Where necessary, support material can be deposited using a separate nozzle, which will be removed by various methods after completion of manufacture. The precision and accuracy of the process are limited by the size of the nozzle, which can have diameters of tenths of millimeters.

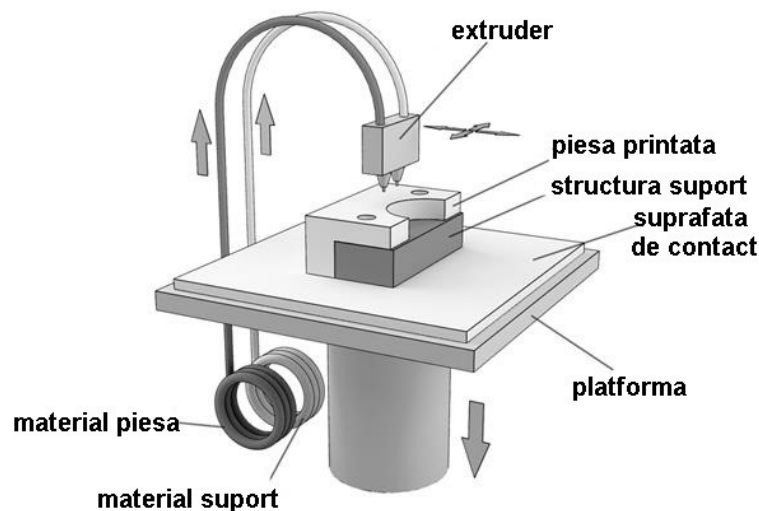


Fig. 2.1. Operating principle of additive manufacturing by fused filament fabrication

Processes that use material extrusion use a relatively simple principle: a material is forced through a cylindrical hole of well-defined dimensions. If the force with which this material is pushed or pulled through the hole is constant, then the characteristics of the resulting material will be constant. In the case of FFF printers, the diameter of the plastic filament remains constant if the nozzle moves at a constant speed that corresponds to the filament feed speed. The extruded material must be in a semi-solid state when passing through the nozzle but must solidify in the form in which it was deposited. In addition, the material must adhere to the previously deposited material layers, as well as to the adjacent areas of the current layer..

Since the material layers are deposited horizontally, the FFF additive manufacturing machine must be able to move in the XoY plane. Moreover, because the areas of certain parts are not always continuous in the horizontal plane, the machine must have the ability to stop the flow of material on demand, in order to traverse areas that do not need to be filled. When one material layer is finalized, the machine must be repositioned on the Z axis in order to start filling

the next layer. Regarding the extrusion process, the most common approach is to use temperature as a way to control the condition of the material. The material is liquefied inside a cavity or a tank, then it is pushed through a nozzle of a predetermined diameter, and will adhere to the previously deposited layer before it solidifies. This process is similar to the extrusion process of polymers, with the difference that the extruder is not mounted horizontally, but vertically..

2.2 FUNDAMENTAL PRINCIPLES OF THE EXTRUSION PROCESS

Additive manufacturing processes that use polymer filament extrusion share several common elements:

- Material loading;
- Material liquifaction (melting);
- Applying pressure to force the material through the nozzle;
- Material extrusion;
- Controlled extruder motion following a predetermined path;
- Material fusion with previously deposited layers and material solidification;
- Use of support or material structures for complex geometric elements.

2.2.2 Material liquifaction (melting)

The extrusion method works due to the fact that once the material arrives in the heated chamber it liquefies and gains a viscosity low enough to be pushed through the nozzle by the pressure imprinted by the feeding mechanism. The chamber in which the liquefaction takes place is usually heated by heating coils by resistive or inductive methods. The heat applied to the material must be constant and must take into account the characteristics of the material, so as not to cause thermal shocks, thermal currents, change of the material phase, etc.

Also, some polymers degrade at high temperatures and the material can burn, leaving residues that are difficult to remove. The solution is to keep the material at a temperature as close as possible to the melting temperature.

2.2.3 Material Extrusion

The extrusion nozzle gives the shape and size of the extruded filament. A larger diameter nozzle allows the material to be extruded easier and faster, but produces a part with lower accuracy and larger deviations from the ideal model (CAD). The diameter of the nozzle also determines the smallest geometric elements that can be created. It is usually recommended that the geometric elements of the parts made by filament deposition are at least twice the diameter of the extrusion nozzle.

Principle of operation: unlike traditional extrusion processes in which the molten material is pushed through the nozzle by a screw, in the case of fused filament fabrication the pressure comes from the filament feeding mechanism. However, the extrusion process can be characterized by drawing a parallel to the simple Archimedean screw extrusion. In the case of the screw model, the molten material moves along the screw channel to the end of the screw where the nozzle is located. The velocity V of the molten material flow along the channel is

$$V = \pi DN \cos \varphi, \quad (2.1)$$

where D is the screw diameter, N is screw rotation speed and φ is the screw angle. Velocity U of the material flow towards the nozzle is:

$$U = \pi DN \sin \varphi. \quad (2.2)$$

For a constant angle of the screw the volumetric flow produced by the screw inside a pipe, also known as the friction flow Q_D is proportional with the dimensions and the rotation speed of the screw

$$QD = D^2NH, \quad (2.3)$$

where H is screw height.

In the case of friction flow the relative speed of the molten material is V for the material in contact with the screw and 0 for the material in contact with the pipe walls. Thus, when the molten material passes through a channel of thickness B and height dy , the flow along the channel Q_D can be expressed as

$$Q_D = \int_0^H \frac{V}{2} B dy = \frac{VBH}{2}. \quad (2.4)$$

Replacing V in the previous equation

$$Q_D = \frac{\pi}{2} DNBH \cos\varphi. \quad (2.5)$$

The pressure in a channel of width L and height H can be derived from the tensile strength equation

$$\tau(x) = \frac{\Delta P}{L} x, \quad (2.6)$$

where x is perpendicular on flow direction and ΔP is the pressure variation along the channel. For Newtonian flows, τ can be expressed as

$$\tau = \eta \frac{dv_z}{dx}, \quad (2.7)$$

where η is the dynamic viscosity of the molten polymer. Combining the two previous equations

$$-\eta \frac{dv_z}{dx} = \frac{\Delta P}{L} dx. \quad (2.8)$$

The average velocity V_m of the molten material moving through a rectangular orifice can be calculated by integrating the above equation between 0 and $\pm H/2$ (center of the channel)

$$V_m = \frac{1}{H} \int_{-\frac{H}{2}}^{\frac{H}{2}} v_z(x) dx = \frac{\Delta PH^2}{12\eta L}. \quad (2.9)$$

Pressure is determined by the flow of material through the channel in a unit of time,

$$Q_P = \frac{BH^3}{12\eta} \cdot \frac{dP}{dz}. \quad (2.10)$$

For extrusion to be possible the condition which needs to be fulfilled is that the pressure on the nozzle should be larger than the pressure on the material

$$Q_T = Q_P - Q_D, \quad (2.11)$$

$$\frac{BH^3}{12\eta} \cdot \frac{dP}{dz} - \frac{VBH}{2} > 0. \quad (2.12)$$

A similar equation can be written for the circular nozzle used in fused filament fabrication. The gripping roller based filament feeding system used by most FFF machines is the one that generates the pressure required for extrusion. If the force exerted by the feeding system is greater than the outlet pressure, the filament may bend on the way to the nozzle. A detailed analysis of the extrusion process in which the feeding is done with a roller system is

made by Turner et al. [22]. This analysis indicates the dependence of the process parameters on those of the extruded material, showing that less brittle materials are more difficult to control during the process. The more flexible the material, the greater the need for precise control of the filament supply to avoid bending the filament.

2.2.4 Material Solidification

Once the material has been extruded, it must retain its original shape, position and dimensions. In practice, many factors change these characteristics, the most important ones being gravity, the surface tension of the molten material and the coefficient of thermal expansion. Often, the expansion and thermal contraction are not linear, which causes deformations of the final part. These can be avoided by precisely controlling the temperature of the chamber in which the material is deposited but also by controlling the cooling process.

It is expected that the extrusion process in the case of additive manufacturing machines will take place through a nozzle with conical inlet and cylindrical outlet. The molten material adheres to the walls of the enclosure where liquefaction takes place, and the velocity of the material in these contact areas is 0. Therefore, the breaking stress equation can be written as

$$\tau = \left(\frac{\dot{\gamma}}{\varphi} \right)^{1/m}, \quad (2.13)$$

where m represents the exponent of the flow and φ is the fluidity of the material. The exponent m represents the flow characteristics for a given material and the deviation from the Newtonian behavior.

2.2.6 Layer adhesion

For heat-based systems, there must be sufficient residual heat in the material to activate the surfaces of the contacting regions, causing adhesion. This process can be viewed as a function of the energy introduced into the material by the extrusion head. If the transmitted energy is insufficient, some regions may have incomplete adhesion and may lead to destruction of the part. Once the material has been extruded, it must solidify and adhere to the previously deposited material. Yardimci et al. defined a series of equations that describe the thermal processes that take place in a filament of extruded material deposited in a given direction x , depending on the properties of the material [23]:

$$\rho \frac{\delta q}{\delta x} = k \frac{\delta^2 T}{\delta x^2} - S_c - S_1, \quad (2.14)$$

where ρ is material density, q is specific enthalpy, k is thermal conductivity, T is the average temperature of the section of the deposited filament. S_c is a factor that describes energy losses through thermal convection

$$S_c = \frac{h}{h_{eff}} (T - T_\infty), \quad (2.15)$$

where h is the thermal convection transfer coefficient and h_{eff} is a geometric factor representing the ratio between the volume of deposited filament and the surface on which thermal convection losses are present. T_∞ temperature is the constant temperature of the environment and k is a term that describes the interaction between adjacent deposited filaments:

$$S_1 = \frac{k}{l^2} (T - T_{adc}), \quad (2.16)$$

where l is the width of the deposited filament and T_{adc} is the temperature of the previously deposited adjacent filament. The purpose of S_1 is to describe the influence of the previously deposited material on the currently deposited filament.

A critical temperature T_c which must be reached for the adhesion process to be activated can be identified. Below this temperature complete and correct adhesion is not possible. We can thus describe a term that expresses the potential of a route to adhere to the rest of the piece as:

$$\varphi = \int_0^t (T - T_c) d\tau. \quad (2.17)$$

2.5 RESEARCH AREAS

2.5.4 Development of processes for additive manufacturing with thermoplastic materials with high processing temperatures

Finding new materials with superior properties that can be used in the manufacture of functional parts is one of the priorities of researchers in the field of additive manufacturing. One of the categories of interest is represented by plastics such as "engineering plastics". Such plastics, such as polyetherimide (PEI) or polyether etherketone (PEEK) are used in industry for both their special mechanical properties and their chemical resistance.

The processing of these materials by additive manufacturing is more difficult than that of commonly used materials. High melting temperatures require the use of specialized components and present difficulties in interacting with the environment during the additive manufacturing process. In this thesis, a series of activities were planned that will allow the formulation of conclusions on additive manufacturing by fused filament fabrication from polymers with high processing temperatures. The plan, shown in Fig. 2.18, includes finite element thermal analysis activities for certain components of a 3D printer, finite element thermal analysis for parts during manufacturing, as well as experimental validation of these analyses. These analyses will be used to establish technical requirements for a vacuum chamber printer and a set of process parameters. Following the construction of the printer, test specimens will be manufactured that will be subjected to destructive and non-destructive testing to determine their mechanical and thermal properties.

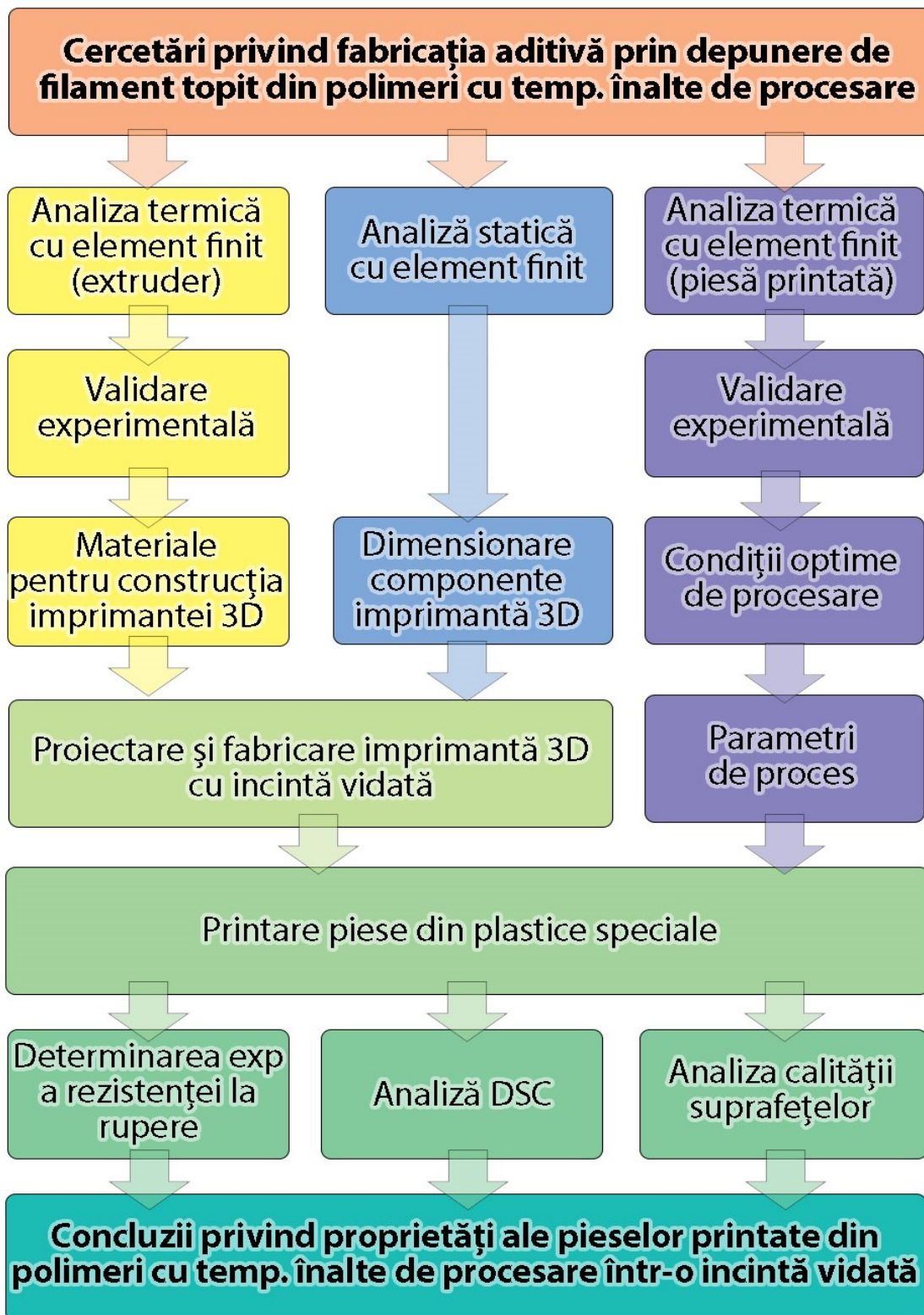


Fig. 2.18. Research activities plan on additive manufacturing by fused filament fabrication from polymers with high processing temperatures

CH. 3 HARDWARE MODELS OF FFF 3D-PRINTERS

From the point of view of the component parts, an additive manufacturing machine using the FFF process can be schematically represented as shown in Fig 3.3.

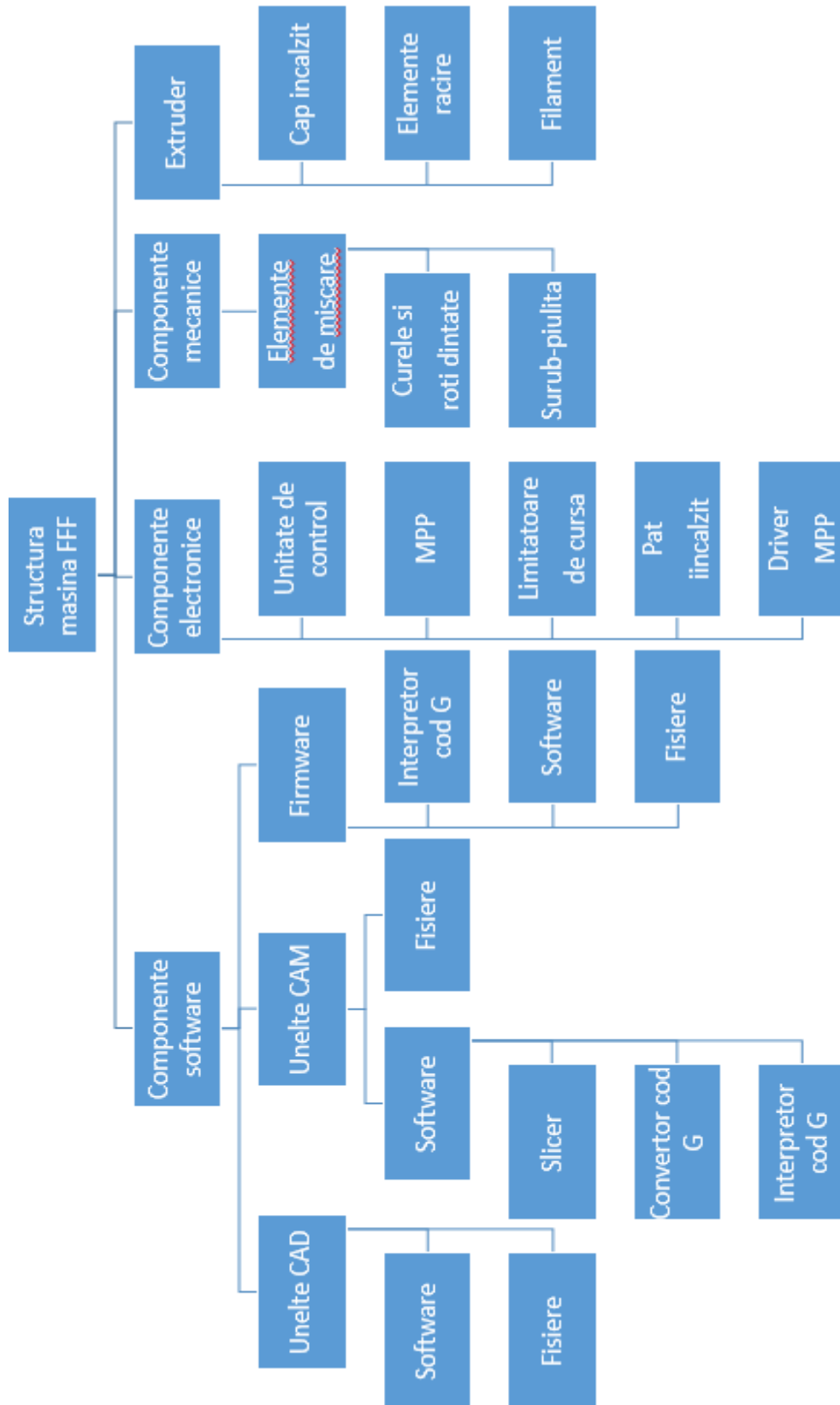


Fig. 3.1. Diagram of the components of an additive manufacturing machine using the FFF process.

CH. 5 PROCESS PARAMETERS

5.1 PROCESS PARAMETERS

During the additive manufacturing process various parameters influence the dimensional accuracy and mechanical properties of the manufactured parts [48], as well as the duration and cost of manufacturing the part. By their nature, these parameters can be divided into different categories:

- Environment parameters:
 - temperature;
 - humidity;
- Position and orientation of parts;
- Extruder selected for part fabrication, on 3D-printers with 2 or more extruders;
- Paramteres specific to the FFF additive manufacturing process:
 - Filament diameter;
 - Extrusion nozzle diameter;
 - Extruder temperature;
 - Machine bed or printing chamber temperature (on 3D printers with heated bed or chamber);
 - Extruder speed;
 - Extruder acceleration;
 - Forced cooling of the printed part;
 - Layer thickness;
 - Layer width;
 - Filament retraction distance;
- Parameters specific to the printed part geometry:
 - Number of outer surface perimeters;
 - Number of outer surface horizontal layers;
- Parameters specific to the material deposition method:
 - Minimum duration for an individual layer (used to ensure adequate cooling);
 - The method of fabricating thin walls;
 - The method of fabricating cylindrical columns;;
 - The method of fabricating islands (disjointed surfaces belonging to the same layer of material).

CH. 6 DETERMINING MATERIALS FOR THE CONSTRUCTION OF AN EXTRUDER FOR POLYMERS WITH HIGH PROCESSING TEMPERATURES USING THERMAL FINITE ELEMENT ANALYSIS

6.1 FINITE ELEMENT ANALYSIS SETUP

The FFF additive manufacturing machine QidiTech Avatar IV uses two extruders equipped with stepper motors, with direct filament feeding by means of a serrated wheel and a tension spring mechanism.

Melting of the filament for extrusion and deposition is achieved by heating an aluminum block using a ceramic cartridge with a power of 40 W. Heat is transferred by thermal conduction to an extrusion nozzle made of brass, with a minimum hole diameter of 0.4 mm. To reduce energy consumption and temperature variations, the aluminum block is wrapped in kapton tape thermal insulation. Temperature monitoring is done with an NTC 3950 thermistor with a resistance of 100 k Ω . The reduction of temperatures outside the melting zone is done by two mechanisms:

- a teflon tube (PTFE), a material with a low thermal conductivity positioned inside the intermediate tube, with the role of reducing the speed of temperature propagation;
- a fan that cools by forced thermal convection a radiator with blades made of aluminum.

For the doctoral project, the extruder nozzle of the 3D printer must reach the temperatures necessary for the melting and extrusion of the materials for which experimental determinations are performed.

For additive manufacturing with PEEK or PPSU material, the extruder nozzle must be maintained at temperatures above 390 °C. From the start, we can note that the temperature monitoring mode with NTC thermistor is not suitable for the application. It is necessary to change this system with PT100 temperature sensors or type K thermocouples. These variants can perform accurate measurements in the 200 ... 400 °C temperature range.

To analyze the thermal performance of the other components, we used a finite element analysis of the temperatures of the extruder components during the manufacturing process. The design of the extruder and of the finite element analysis were initially validated by analysing the performance of the extruder with the parameters recommended by the manufacturer. Then, we resorted to thermal analysis for a case in which the ceramic heating element raises the nozzle temperature to 400 °C. Subsequently, since the only cooling parameter that can be adjusted without changing the mechanical structure of the extruder is the airflow speed generated by the fan, the thermal analysis was repeated with different values of cooling generated by forced thermal convection [34].

The thermal behavior of the extruder during the additive manufacturing process results from the combination of two heat transfer mechanisms. In the first phase, the extrusion nozzle is heated by the ceramic cartridge integrated in the aluminum block. Subsequently, the heat is dissipated from the extruder body by forced convection. A finite element analysis was designed to analyze the thermal performance of the extruder during the extrusion process, depending on the air velocity generated by the extruder fan [68]. The 3D virtual model was created in the SolidWorks 2011 software package (Fig. 6.2).

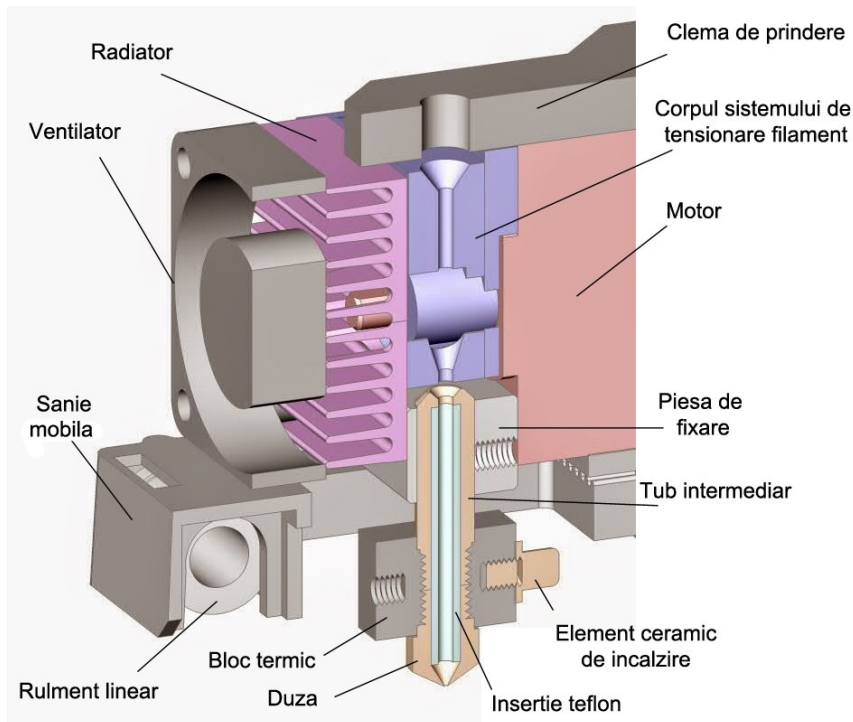


Fig. 6.2. Section through the 3D virtual model of the carriage which holds the extruder

This 3D model has been simplified by removing small threads and chamfers, and has been imported into the thermal simulation module of the same software package.

The assembly consists of 6 components subjected to thermal analysis (Fig. 6.3), as follows:

1. Thermal block made of aluminum AW 3003-H18, which contains 2 cylindrical holes, one for the ceramic heating cartridge and the second for the thermistor;
2. Extrusion nozzle (brass EN CW614N);
3. Intermediary steel tube;
4. Heatbreak tube made from teflon (PTFE);
5. Extruder mounting bracket (aluminum AW 3003-H18);
6. Fin radiator (aluminum 6063).

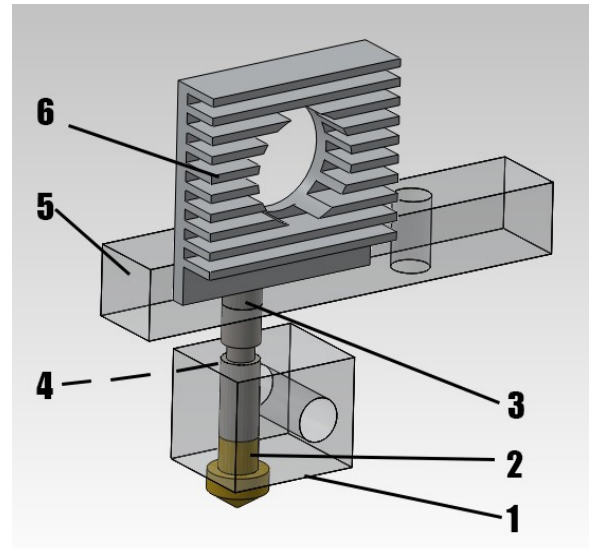


Fig. 6.3. Simplified virtual model subjected to thermal analysis

In the case of solid parts, thermal analysis solves the energy equation for every node

$$\rho C_p u \cdot \nabla T = \nabla \cdot (k \nabla T) + \dot{Q}, \quad (6.1)$$

where C_p is heat capacity at constant pressure;

k is thermal conductivity,

Q is the heat flow.

The conditions setup in the thermal analysis (Fig. 6.4):

- All items declared in the thermal analysis are considered thermally insulated from the environment; the only element that introduces energy into the system is considered the ceramic heating element;
- The energy is taken out of the system through thermal convection;
- The contact between the air and the walls of the extruder takes into account the no-slip condition, which means that the air speed is equal to zero at the contact surface;
- Although the fan is not included in the model, its influence is included in the thermal analysis by the convection heat transfer variable. In the case of the analysis of the behavior at high temperature, 3 values of the air speed given by the fan were analyzed by considering 3 values for the variable of thermal transfer by convection: 25 W, 50 W or 100 W / (m²K), respectively [57];
- For the aluminum mounting bracket and the exposed surface of the intermediate steel tube, as well as for the inner cylindrical surface of the heatbreak, a heat transfer factor by free convection with the air of 25 W/(m²K);
- As the thermal block is insulated using Kapton tape, energy losses through contact with the environment are neglected; In the analyzed model, the thermal block is considered insulated;
- Thermal energy is introduced into the system through the cylindrical surface in contact with the ceramic heating element. A constant temperature has been declared for this surface, as follows:
 - for the validation analysis of the virtual model, $t = 230\text{ °C}$
 - for the analysis of high temperature behavior, $t = 400\text{ °C}$
- Starting conditions:
 - Constant pressure of 1 atm.
 - Temperature of the air that comes in contact with the surface of the extruder is room temperature, 20 °C.

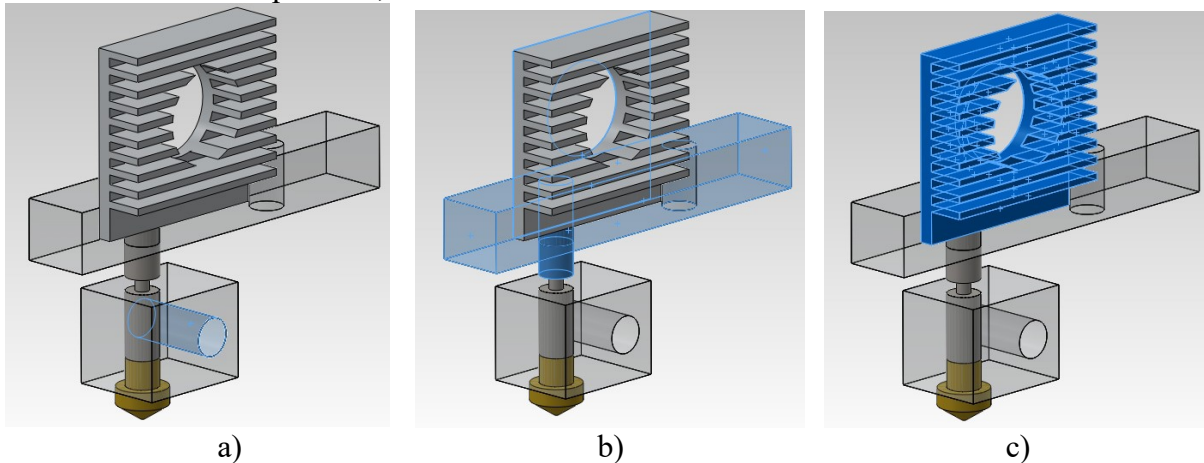


Fig. 6.4. Application of thermal loads a) Constant temperature, b) Free convection; c) Forced convection

Meshing of the components was done with the Fine setting, setting the minimum element size of 0.1 mm. The maximum size of the elements is 1 mm.

6.2 RESULTS OF THE FINITE ELEMENT ANALYSIS

Following the thermal finite element analysis (Fig. 6.6), it can be seen that the temperatures in the case of the validation analysis fall within the normal limits. The maximum temperature reached by the teflon tube (Fig. 6.7) is 228.31 °C, under the limit of 250 °C.

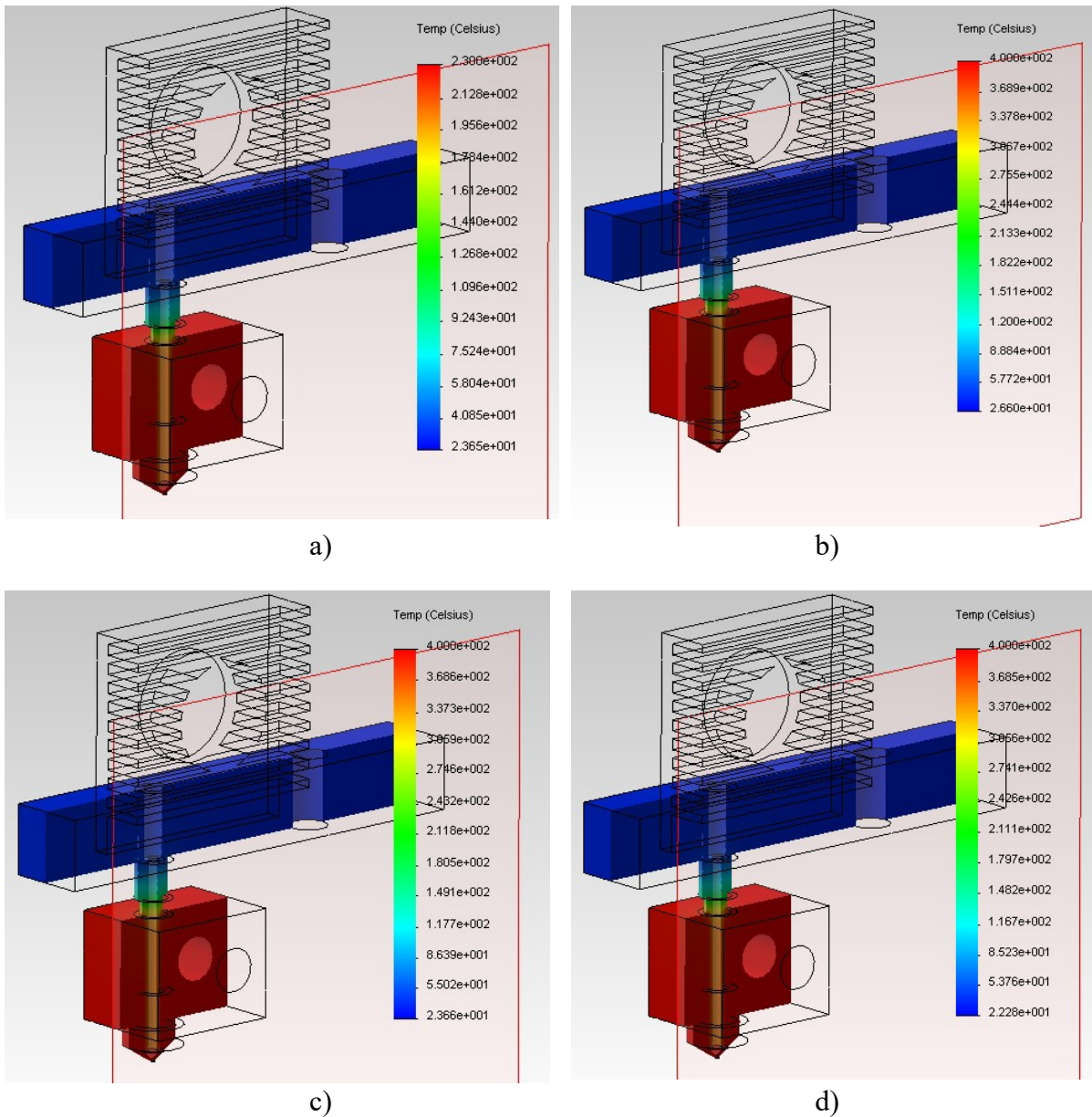


Fig. 6.6. Finite element analysis results: a) 230 °C, with fan at maximum speed; b) 400 °C, with fan turned off; c) 400 °C, with fan at medium speed; d) 400 °C, with fan at maximum speed.

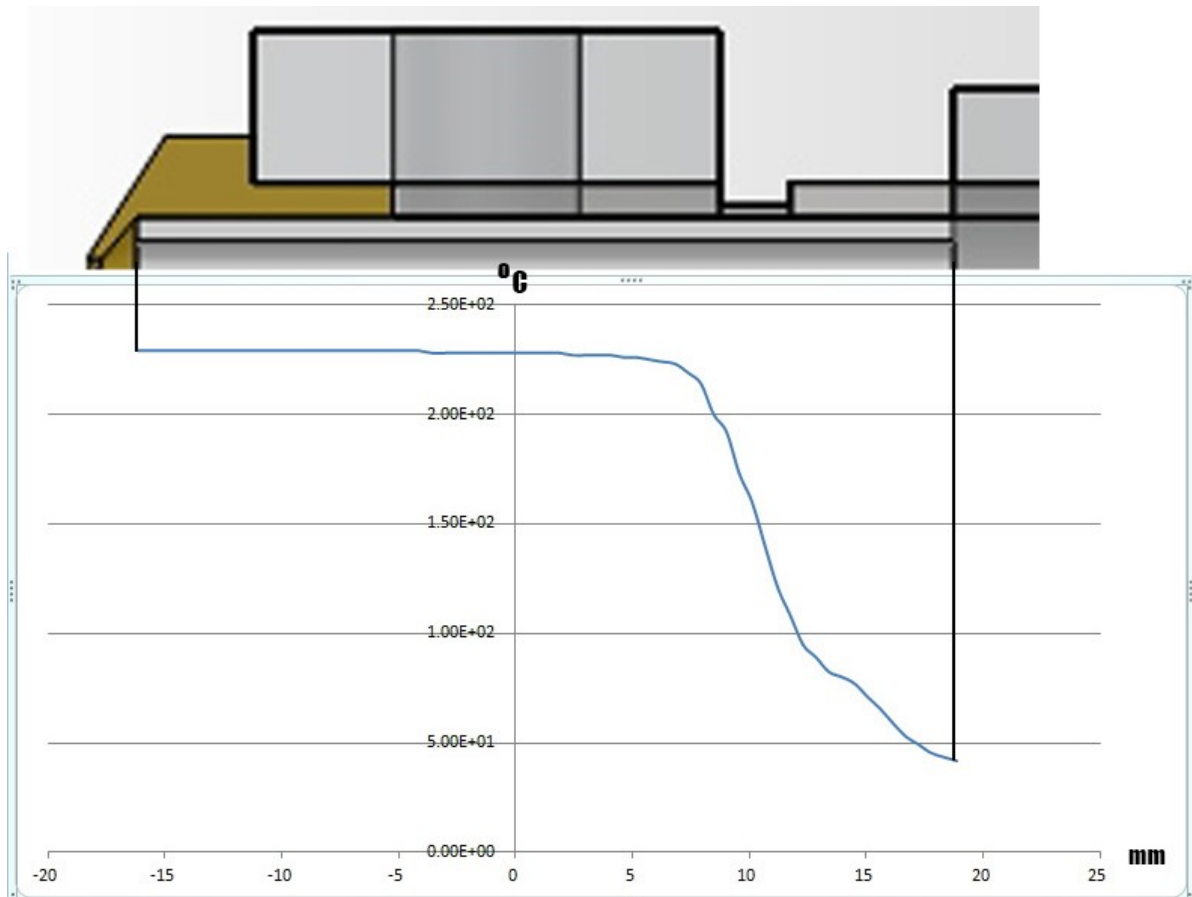


Fig. 6.7. Temperature distribution along the teflon tube during validation analysis

Following the high temperature analysis (Fig. 6.8), in which the aluminum block in which the heating ceramic cartridge is positioned was brought to a temperature of 400 °C, it can be seen that the temperature of the teflon heatbreak has passed the admissible temperature of 250 °C in more than 72% of the tube's volume. It can also be seen that the impact of increasing the fan speed is small, as it is positioned at a long distance from the melting zone [86].

Experimental data show that replacing the radiator with another more efficient construction variant would not produce significant changes [70].

Another problem is the temperature reached by the aluminum thermal block. According to available experimental data, the mechanical strength of AW-3003-H18 aluminum decreases from 190 MPa at 20 °C to only 21 MPa at 400 °C.

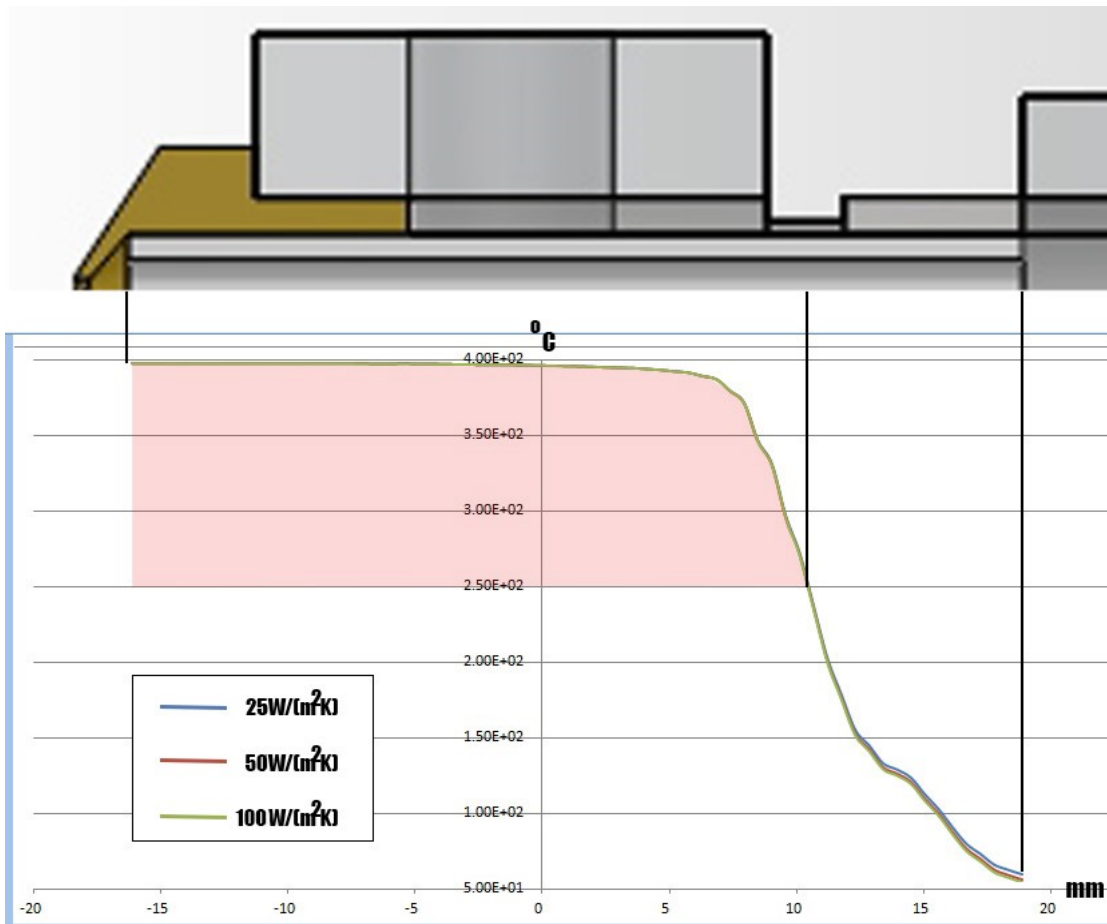


Fig. 6.8. Temperature distribution along the teflon tube during high temperature analysis

Also, the brass (EN CW614N) nozzle exceeds the maximum continuous operating temperature, having a mechanical strength of 51 MPa at 400 °C.

The other components, namely the aluminum mounting bracket AW-3003-H18, the 6063 aluminum radiator and the steel intermediate tube maintained temperatures below the maximum continuous operating temperatures.

Next, the thermal analysis was repeated after the replacement of the incompatible components according to Table 6.6. and Fig. 6.10.

Table 6.6. Component revision

No..	Component	Change
1	Nozzle	Material changed from brass EN CW614N to 304 stainless steel
2	Thermal block	Material changed from aluminum AW-3003-H18 to 304 stainless steel
3	Teflon heatbreak	The two components were redesigned into a single component
4	Intermediary steel tube	made from 304 stainless steel

After repeating the thermal analysis it can be seen that all components fall within the temperature limits (Fig. 6.11, Table 6.7).

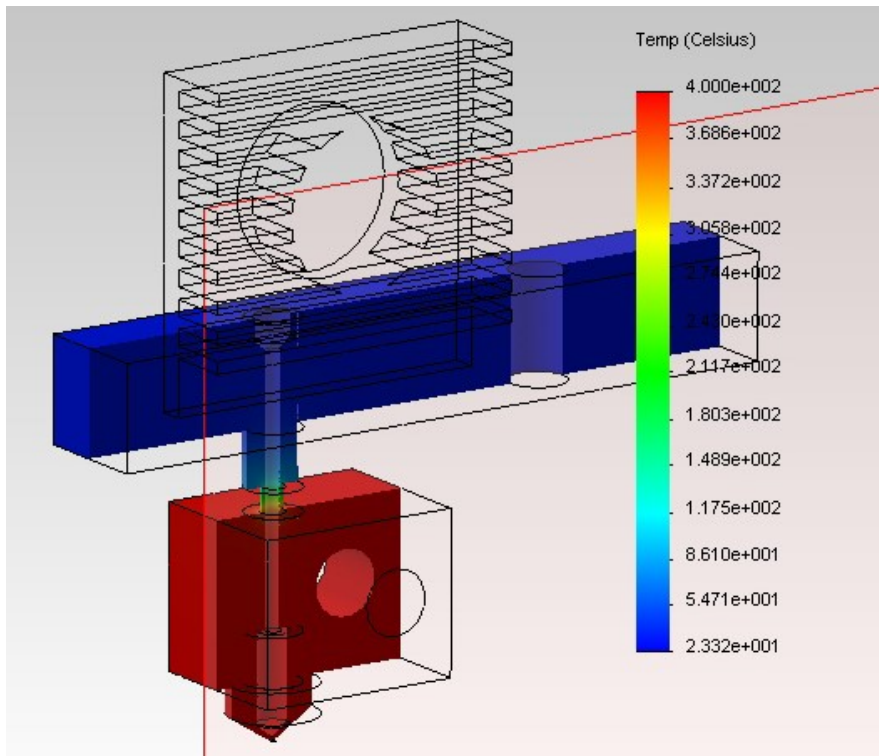


Fig. 6.11. Results of the thermal finite element analysis after the revision of components

Table 6.7. Maximum temperatures reached after component redesign.

No.	Component	Maximum temperature [°C]
1	Thermal block	400
2	Extrusion nozzle	399.21
3	Combined heatbreak	398.67
4	Monting bracket	57.31
5	Fin radiator	39.84

6.3 EXPERIMENTAL DETERMINATION OF THE OPERATING TEMPERATURES OF AN EXTRUDER FOR ADDITIVE MANUFACTURING BY FUSED FILAMENT FABRICATION

The first part of this chapter treated the problem of the materials used to make the extruder of an additive manufacturing machine. The thermal behavior of an MK10 extruder was analyzed using a finite element analysis method (static thermal analysis) and conclusions were drawn regarding the behavior of the extruder at temperatures between 230 °C and 400 °C. In the following section the transient thermal analysis will be presented, as well as the experimental validation of the results obtained from the finite element analysis. The process was repeated for a new type of extruder whose construction takes into account the conclusions formulated following the previous static thermal analysis.

Thermistor type temperature sensors were used to determine the temperatures. These are circuit elements that change their resistance depending on the temperature. The type of thermistors used is NTC 3950, with a resistance of 100 kΩ at a temperature of 21 °C. The experimental arrangement consists of 5 thermistors connected to a measuring circuit and an Arduino type micro-controller. After attaching the sensors to the extruder, the printer was used to print a test piece whose manufacturing process took 15 minutes, long enough for the extruder

components to reach thermal equilibrium. Temperatures from measurements and data processing were saved in text files, from where they were uploaded to Microsoft Excel to create charts.

The finite element analysis of the MK10 extruder was performed using SolidWorks Flow Simulation and incorporates elements of transient thermal analysis and fluid dynamics. The conditions specified in the finite element analysis are:

- temperature 230 °C for the cylindrical surface in which the ceramic cartridge is fixed (Fig. 6.14a)
- thermal convection 25 W/m²K for the lamellar surface of the radiator (Fig. 6.14b); the air hitting this surface has room temperature, 25 °C.
- thermal convection 20 W/m²K for the exposed surface of the intermediate tube; the air that comes in contact with this surface has a temperature of 45°C.
- fluid flow (air) set as lamellar and turbulent;
- the initial temperature of the extruder parts is room temperature, 25 °C
- the total duration of the transient thermal analysis is 900 seconds, with the calculation of intermediate solutions once per second.

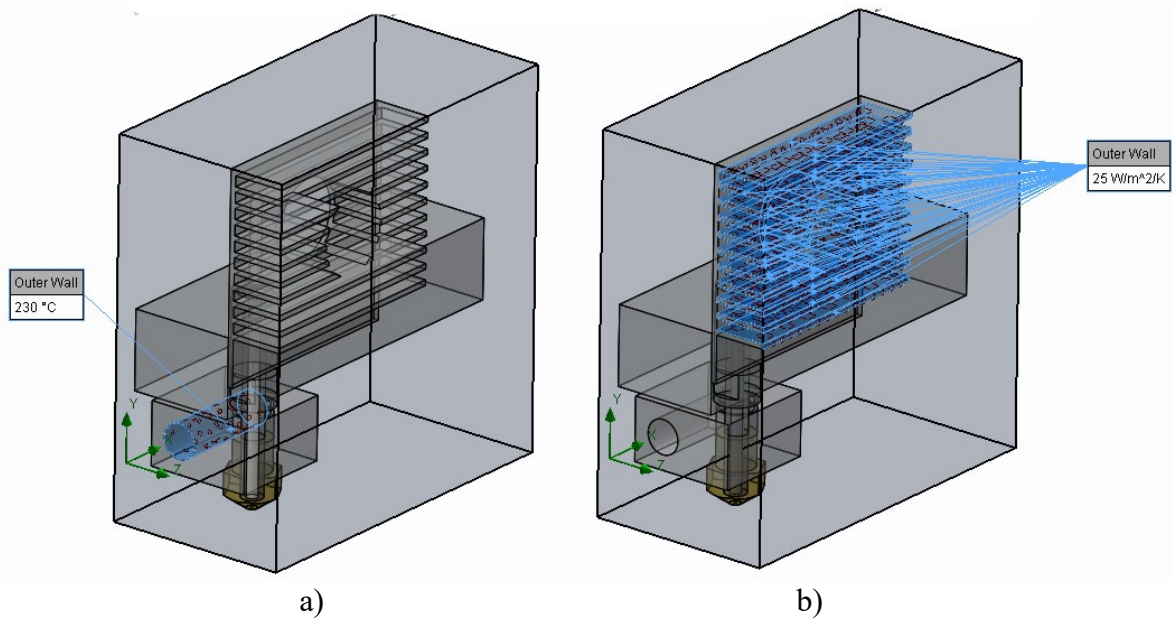


Fig. 6.14. a) Ceramic cartridge temperature; b) Heat transfer on the radiator surface

The results of the finite element thermal analysis, as well as the experimental measurements performed for the MK10 type extruder are presented in Fig. 6.15.

The position of the temperature sensors and the experimental values measured with their help can be found in Table 6.10.

Table 6.10. Experimental values measured for the MK10 extruder

Sensor No.	Placement	Distance from nozzle tip [mm]	Stable temperature [°C]
1	Exposed bottom side of the intermediary tube	19,0	205,62
2	Exposed upper part of the intermediate tube	25,0	135,52
3	Center of the bracket	32,5	138,17
4	The bottom of the radiator	40,0	125,12
5	Center of the radiator	55,0	122,76

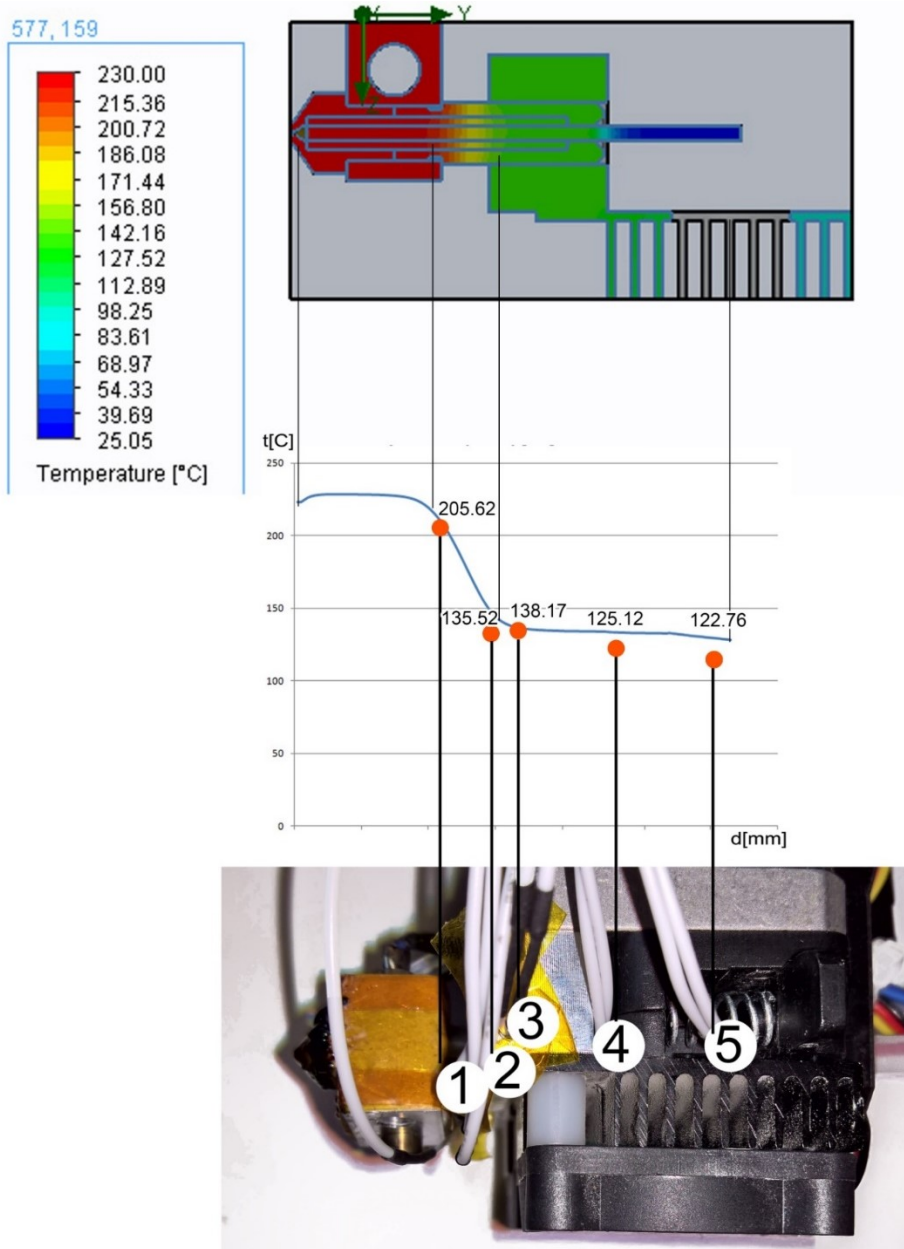


Fig. 6.15. Experimental temperature measurements of the MK10 extruder

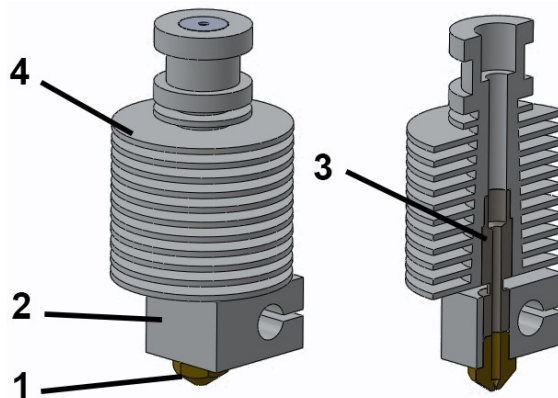


Fig. 6.16. Improved extruder components. 1) extrusion nozzle (brass EN CW614N); 2) thermal block (aluminum AW-3003-H18); 3) connection tube (SS304); 4) cylindrical radiator (aluminum 6063).

The conditions specified in the finite element analysis are:

- the geometry and materials specified in the figure 6.16;
- temperature 230 °C for the cylindrical surface in which the ceramic cartridge is fixed (Fig. 6.17a)
- thermal convection 25 W/m²K for the lamellar surface of the radiator (Fig. 6.17b); the air hitting this surface has room temperature, 25 °C.
- fluid flow (air) set as lamellar and turbulent;
- the initial temperature of the extruder parts is room temperature, 25 °C
- the total duration of the transient thermal analysis is 900 seconds, with the calculation of intermediate solutions once per second.

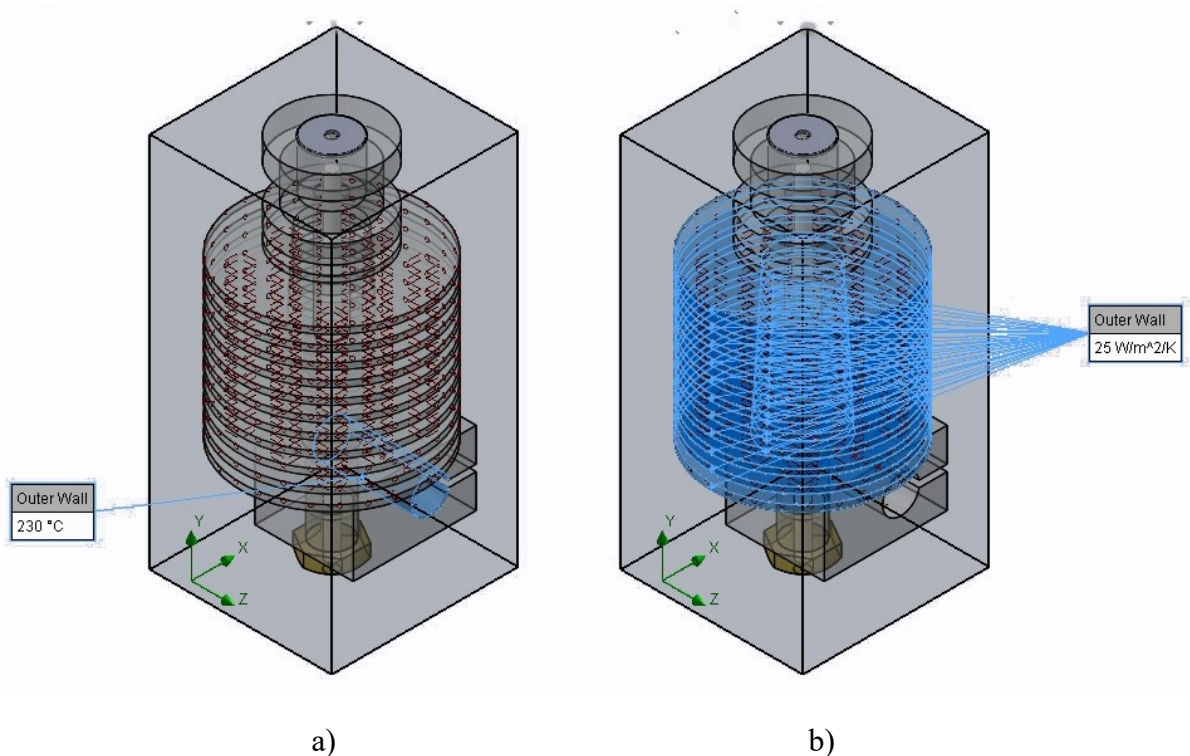


Fig. 6.17. a) Definition of ceramic cartridge temperature; b) Definition of heat transfer on the radiator surface

The results of the thermal analysis with finite elements, as well as the experimental measurements performed for the extruder made entirely of metal are presented in Fig. 6.18.

The position of the temperature sensors and the experimental values measured with their help can be found in Table 6.12.

Table 6.12. Experimental values measured for the all-metal extruder

Sensor No.	Placement	Distance from nozzle tip [mm]	Stable temperature [°C]
1	Exposed bottom of the intermediate tube	16,5	223,72
2	Exposed upper part of the intermediate tube	18,5	62,97
3	Lower third of the radiator	21	62,54
4	Center of the radiator	28,5	53,20
5	Upper third of the radiator	38,5	49,33

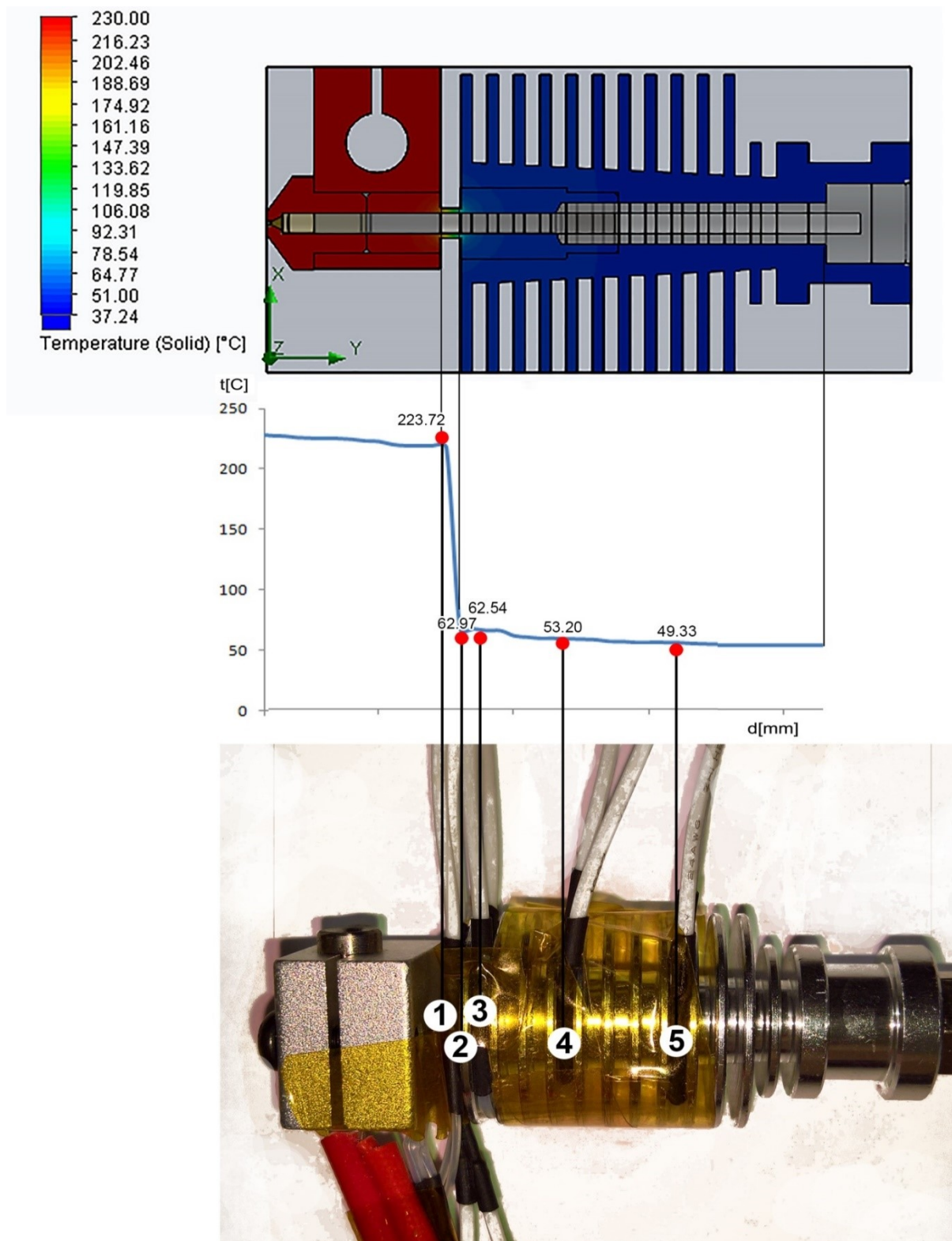


Fig. 6.18. Experimental temperature measurements of the all-metal extruder

6.4 THERMAL FINITE ELEMENT ANALYSIS OF A PART MANUFACTURED BY FUSED FILAMENT FABRICATION

A finite element analysis was performed in order to determine the influence of the process parameters on the thermal behavior of the parts manufactured by fused filament fabrication.

The literature presents different methods [71, 72] for thermal simulation of the additive manufacturing process. Most approaches use individual discretization of filaments of material deposited in various positions (sideways, above) and analyze the distribution of temperatures according to the position and time of their deposition [73]. While this approach produces accurate results at the level of individual filaments, the generalization of the method for simulating the behavior of a complete part presents difficulties [74]:

- during the additive manufacturing process, the filament deposition position varies depending on the surface of the deposited layer.
- the direction of deposition differs depending on the default process parameters, specific to the software program that generates the deposition trajectory.

In what follows, another approach is proposed, namely a simplified analysis, at macro level, in which the analyzed part is manufactured layer by layer, and the analysis with finite elements is done for each individual layer. The simulation process is performed in steps (Fig. 6.19):

1. Establishing process parameters
 - Deposition speed;
 - Material layer height;
 - Deposited filament width;
 - Extrusion temperature;
 - Build plate or chamber temperature (ambient air temperature).
2. Sectioning the part in layers accounting for material layer height.
3. Taking into account the deposition rate, the horizontal move speed and the width of the deposited material filament, the time required for the deposition of a layer is approximated. Part infill is considered to be 100%.
4. The thermal evolution of the top layer of deposited material is approximated while taking into account the temperature of the extruder.
5. The temperature of the base layer is approximately equal to the temperature of the heated bed.
6. After setting the thermal parameters, the dynamic thermal analysis for the first two deposited layers is performed, where the initial temperature of the lower layer is that set in step 5, and the initial temperature of the upper layer is that determined in step 4.
7. The transient thermal analysis is run for a period of time equal to the time required to deposit a layer determined in step 3.
8. The temperatures resulting from the dynamic analysis are saved and are considered as initial temperatures for the next simulation. The process is repeated until all layers of material are analyzed.

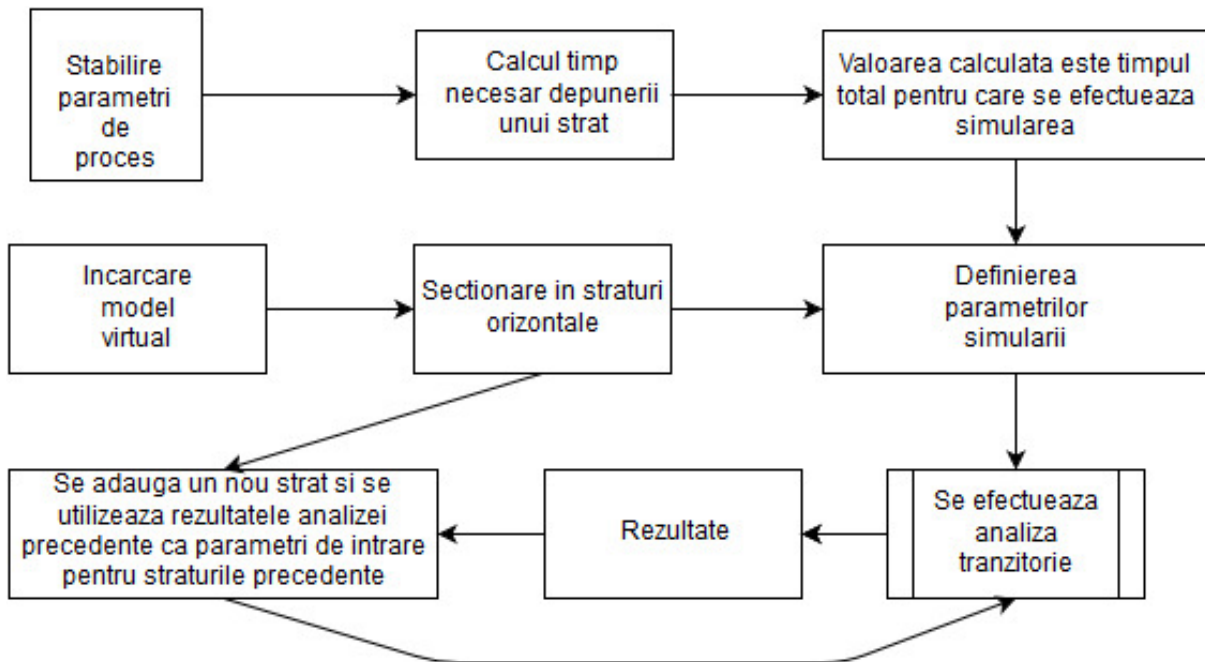


Fig. 6.19. Diagram of the stages of the thermal analysis

The tested piece is a parallelepiped with dimensions $20 \times 20 \times 40$ mm, sectioned in 200 layers of material, each with a thickness of 0.2 mm. Using the estimates provided by the software dedicated to the sectioning of virtual models for additive manufacturing, the approximate time of deposition of a layer of material was calculated taking into account the process parameters: deposition speed 60 mm / s, filament width 0.4 mm. The calculated time is 20 seconds for each deposited layer. Therefore, the total simulation time is 4000 seconds. The parameters used in the finite element analysis can be found in Table 6.13.

Table 6.13. Thermal parameters used in finite element analysis

No..	Parameter	Value
1	Thermal conductivity of PLA	0.10 W/mK
2	Thermal conductivity of ABS	0.16 W/mK
3	Thermal conductivity of PETG	0.39 W/mK
4	Thermal transfer coeff. of air	25 W/m ² K
5	Ambient temperature in open printing chamber	25 °C
6	Ambient temperature in open printing chamber	45 °C
7	Extruder temperature	190-230 °C
8	Heated bed temperature	25-110 °C

Fig. 6.20 presents the results of the transient thermal analysis for the first 5 cycles of the analysis and the temperature distribution for each of them. The measurements are recorded in the time moments presented in Table 6.14.

Table 6.14.

Cicle No.	Part Height [mm]	Analysis Time
1	1	1'40"
2	2	3'20"
3	3	5'00"
4	4	6'40"
5	5	8'20"

From the transient thermal analysis it can be seen that the temperature of the deposited layers decreases rapidly following exposure to the environment at room temperature. The cooling of the part is more accentuated towards the external surfaces, especially around the edges of the part. After the completion of the second cycle it can be seen that the part has cooled enough that the highest temperatures are recorded around the bed heated to 60 °C. When adding subsequent layers of material, the formation of a warm area inside the part is observed.

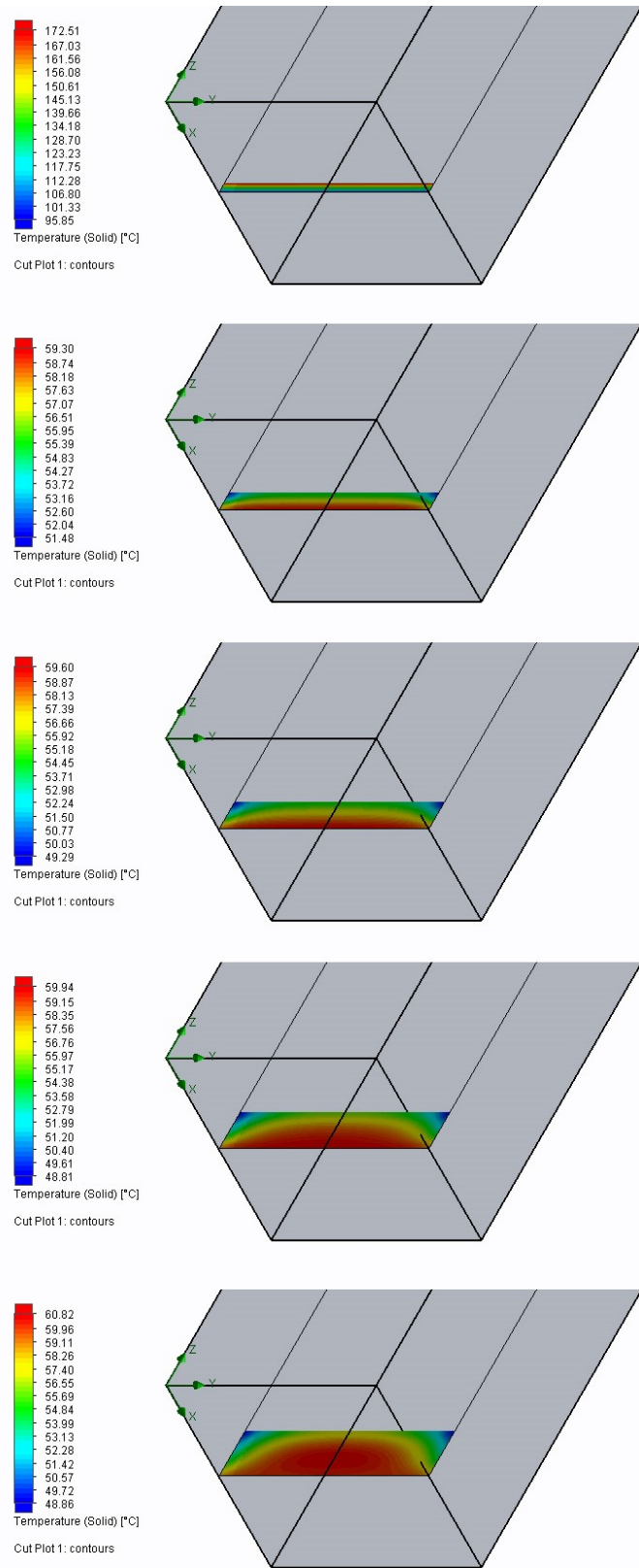


Fig. 6.20. The first 5 cycles of thermal analysis

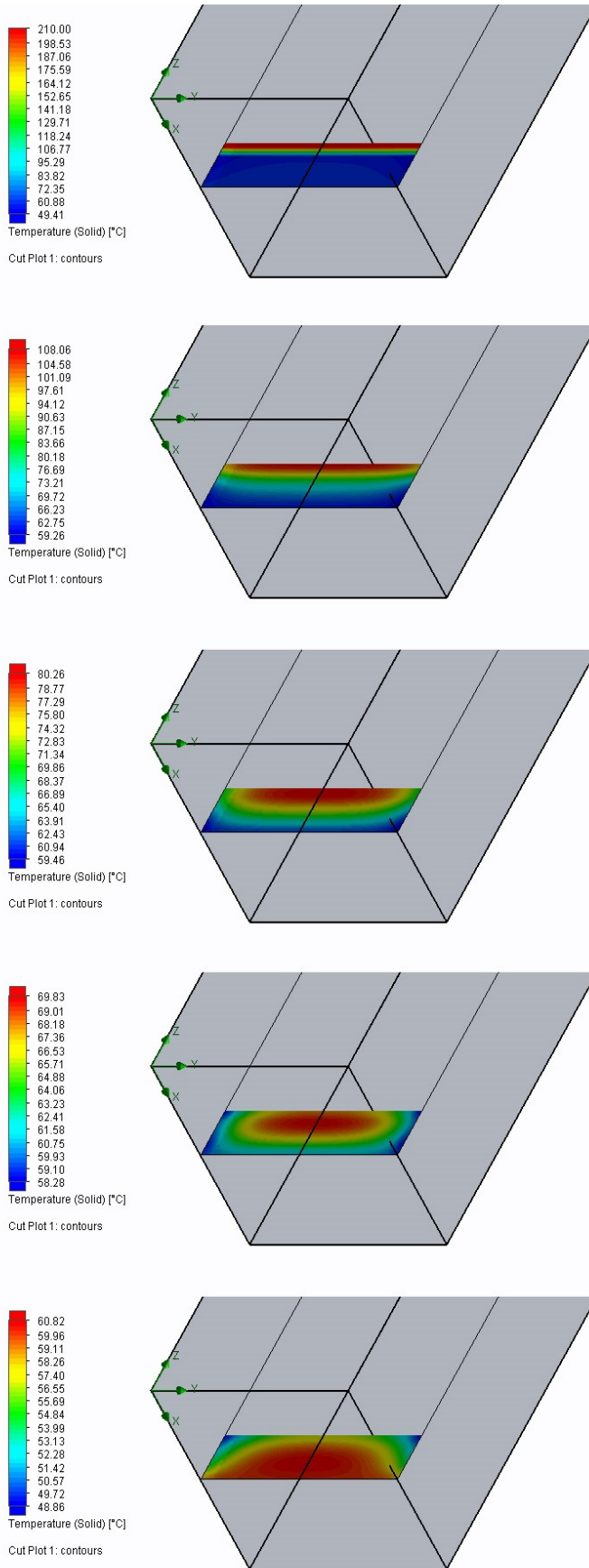


Fig. 6.21 shows the evolution over time of temperatures in the same simulation cycle. The first image represents the moment $t = 0$ of the deposition of a new layer of material, and in the adjacent images it can be observed the way in which the heat is distributed (Table 6.15).

Table 6.15

Cicle No.	Part Height [mm]	Analysis Time
5	5	6'40"
5	5	7'00"
5	5	7'20"
5	5	7'40"
5	5	8'00"

It should be noted that the temperature inside the piece reaches the temperature of the bed before completing the cycle and the deposition of the next layer, while cooling in areas closer to the surface is more pronounced. This indicates the presence of temperature fluctuations, which leads to the accumulation of internal voltages. In the upper part of the part the temperatures fall below the temperature of the bed heated to $60\text{ }^{\circ}\text{C}$, indicating a low influence of the heated bed for the upper part of the part, even in the case of small parts ($z = 5\text{ mm}$).

Fig. 6.21. Temperature evolution in the 5th cycle of thermal analysis

Fig. 6.22 presents the situation of the part in an advanced stage of the manufacturing process.

The first image in the sequence represents the moment t_0 of the deposition of the layer $z = 30$ mm, and the subsequent images illustrate the way heat propagates in the part.

Table 6.16

Cicle No.	Part Height [mm]	Analysis Time
30	30	48'40"
30	30	49'00"
30	30	49'20"
30	30	49'40"
30	30	50'00"

As it can be seen, the influence of the heated bed at this point in the manufacturing process is reduced to the lower section of the part, the side surfaces reaching a temperature of 31.56°C .

Thus, it can be concluded that, starting from a certain distance of the currently deposited layer from the plane of the heated bed, the effect of the latter is too low to justify maintaining its temperature at an elevated level. Since the heated bed is one of the main consumers of electricity of a 3D printer equipped with such a system, by lowering its temperature starting with a certain point of the printing process, manufacturing costs can be reduced. The efficiency of such a change is increased in the case of tall parts.

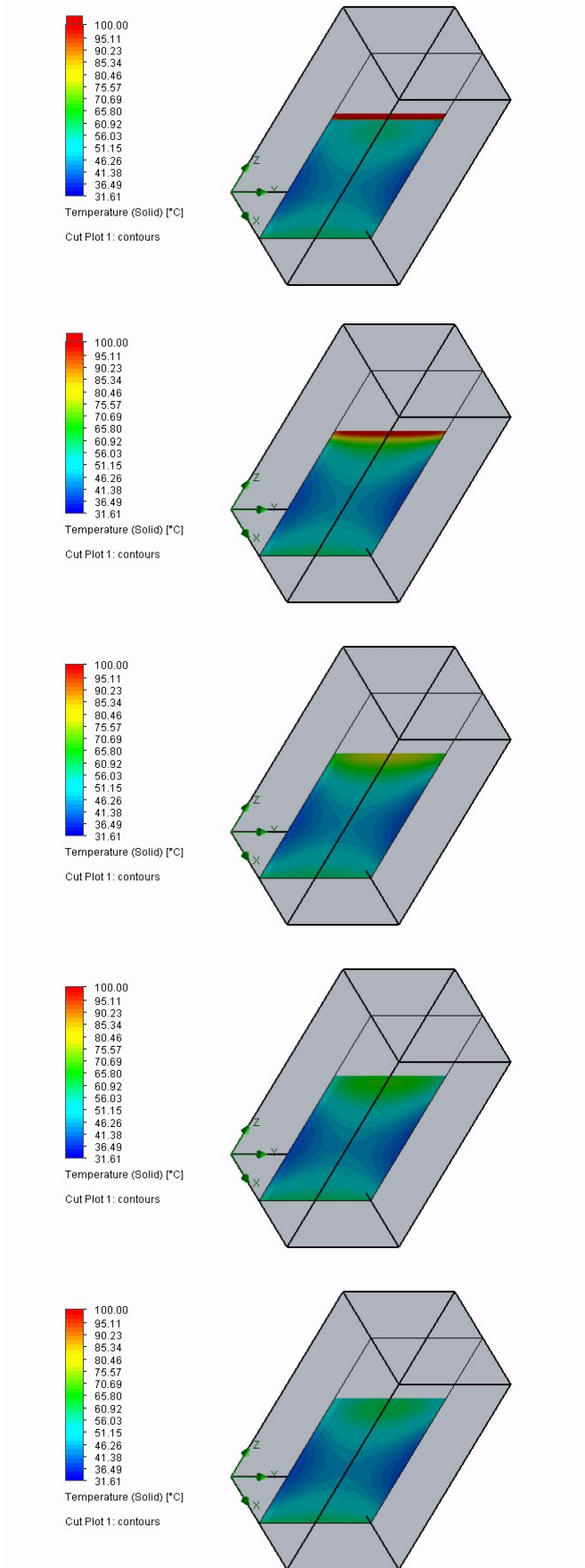


Fig. 6.22. Temperature evolution in the 30th cycle of thermal analysis

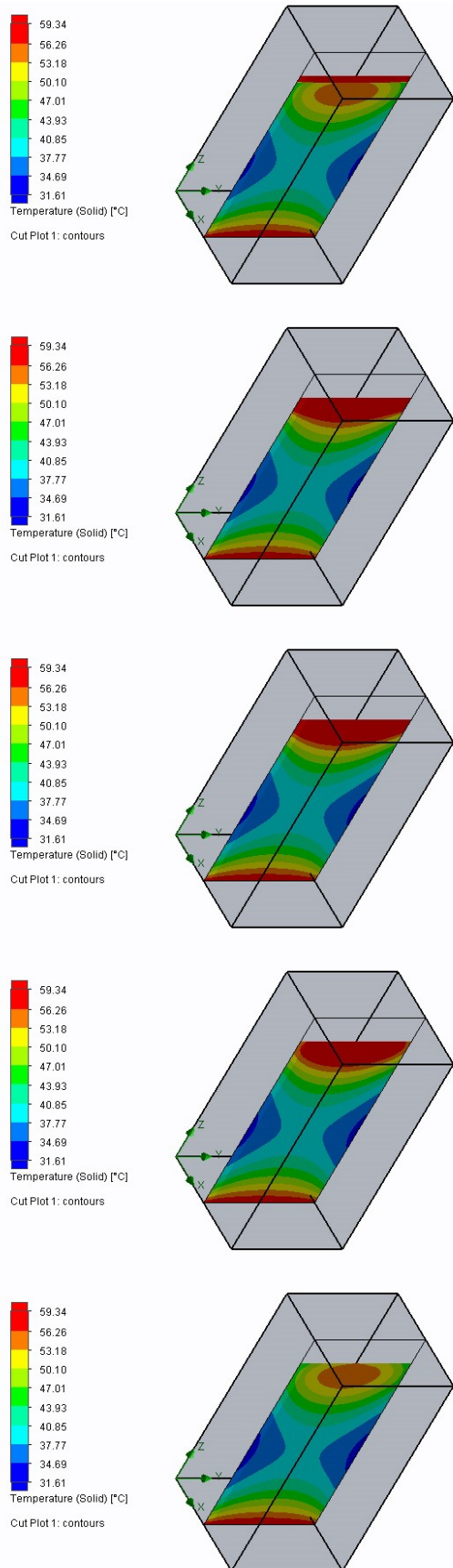


Fig. 6.23 presents 5 sequences from the simulation captured at the time of deposition of a layer of molten material at a distance $z = 35$ mm from the base of the part (Table 6.17).

Table 6.17

Cicle No.	Part Height [mm]	Analysis Time
35	35	58'20"
35	35	58'40"
35	35	59'00"
35	35	59'20"
35	35	59'40"

The scale of the section graphs was fixed to show temperatures between 31.61 °C and 59.34 °C, to highlight the way heat propagation occurs.

Fig. 6.23. Thermal analysis: temperature distribution when depositing a layer at a part height of $z = 35$ mm

6.5 EXPERIMENTAL MEASUREMENT OF INTERIOR TEMPERATURE OF PARTS MADE BY FUSED FILAMENT FABRICATION

To validate the results obtained based on the finite element thermal analysis model described above, as well as to identify the influence of various thermal parameters on the heat propagation mode in the manufactured part, a number of tests were performed, manufacturing test pieces of $20 \times 20 \times 40$ mm from the 3 materials specified above. The test pieces were provided with 5 cylindrical bores (Fig. 6.25) positioned 5 mm from the base of the piece.

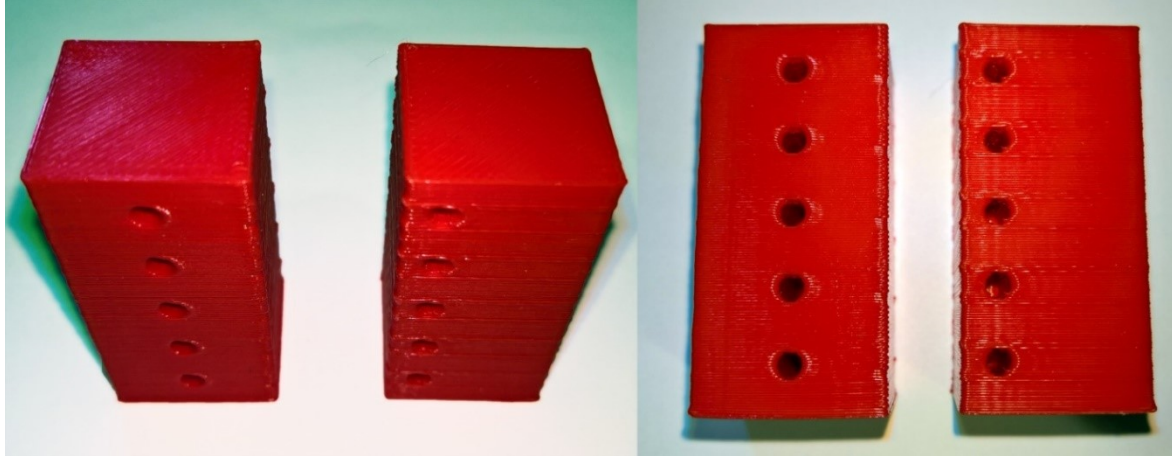


Fig. 6.25. Test pieces manufactured for experimental temperature measurement

The bores were arranged equidistantly in the vertical direction, at a distance of 7.5 mm from each other. Two positions in the vertical plane were considered, namely: a position in the plane of symmetry of the part and a position halfway between the plane of symmetry and the outer surface of the part. Table 6.19 lists the coordinates of the points whose temperature was determined experimentally. The point of origin of the part is considered to be the intersection of the frontal plane with the left lateral plane and the base plane.

Table 6.19. Coordinates of experimentally determined points

Point No.	Coordinates (X;Y;Z)
P1	(10;10;5)
P2	(10;10;12,5)
P3	(10;10;20)
P4	(10;10;27,5)
P5	(10;10;35)
P6	(5;10;5)
P7	(5;10;12,5)
P8	(5;10;20)
P9	(5;10;27,5)
P10	(5;10;35)

During manufacturing, once the layer delimiting the inner bores was completed, temperature sensors were inserted in the part to monitor the cooling process (Fig. 6.26). The parts were manufactured using a QidiTech Avatar IV 3D printer equipped with the MK10 extruder.

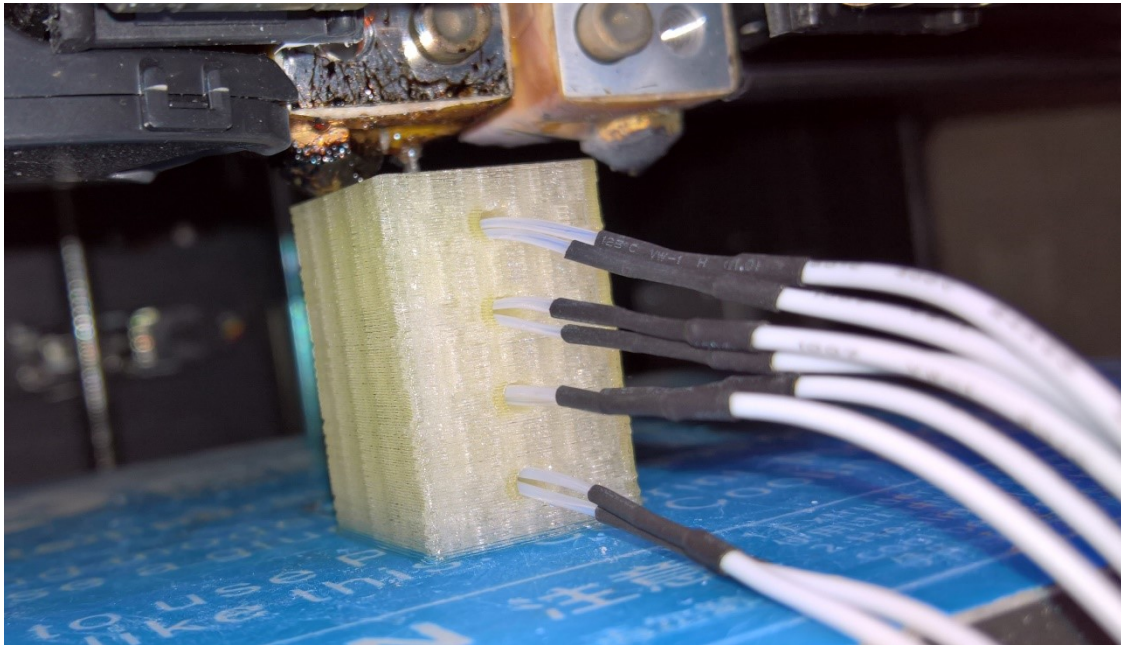


Fig. 6.26. Positioning the temperature sensors inside the part

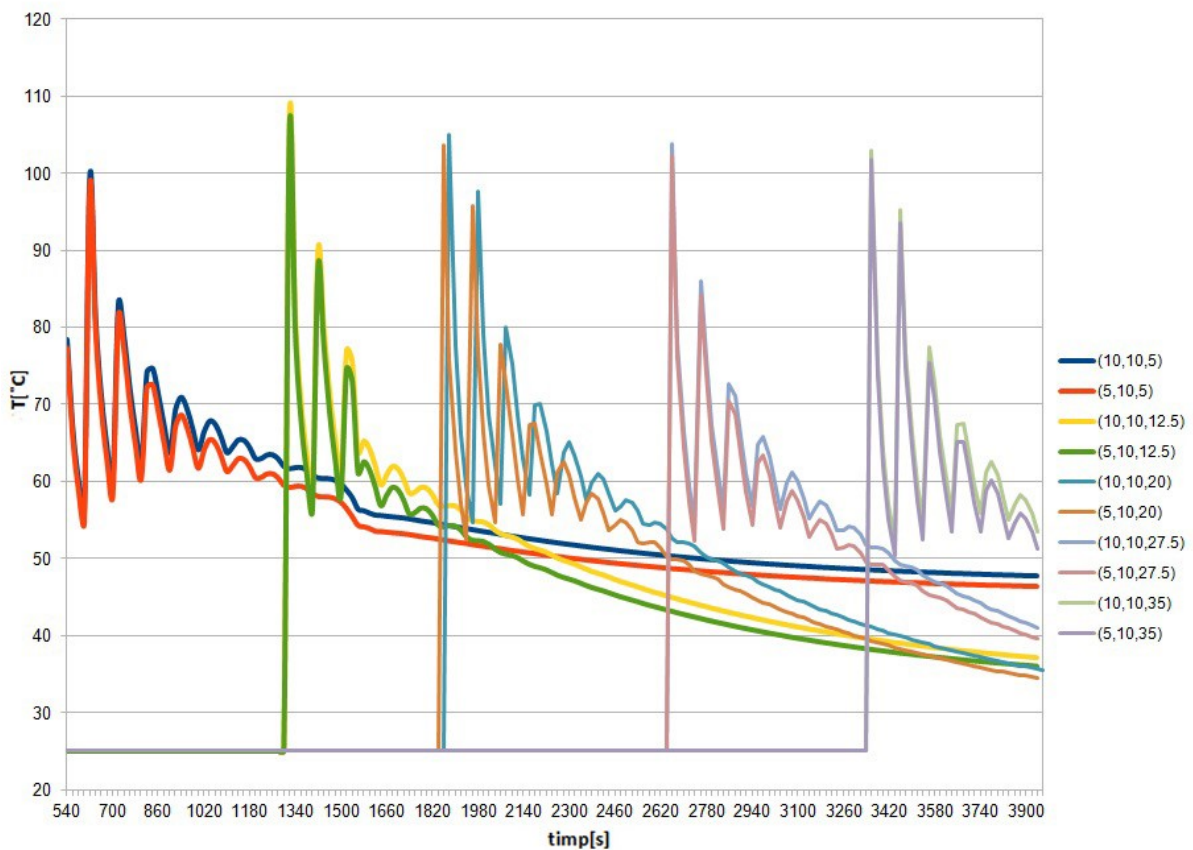


Fig. 6.28. Temperature variation during the additive manufacturing process (5 sensors)

In Fig. 6.28 experimental results are plotted for two test parts made with PLA material at a printing temperature of 210 °C and a deposition rate of 60 mm / s. The time interval in which the experimental data are taken is between 540 and 4000 seconds for the first temperature sensor, between 1280 and 4000 seconds for the 2nd temperature sensor, between 1820 s and

4000 s for the third temperature sensor, between 2640 s and 4000 s for the fourth temperature sensor and between 3300 s and 4000 s for the fifth temperature sensor..

The graphically represented values are the measured values for both points in the same horizontal plane

As the measured point moves away from the heated bed, it should be noted that the temperature variations are more pronounced initially, but decrease more rapidly as the process progresses. This difference in the thermal behavior of the part is useful in determining the areas where internal stresses may occur.

The graph in Fig. 6.29 shows the temperature differences between the pairs of points in the horizontal plane. In the case of the part made of PLA at a temperature of 210 °C, these differences are at most 2.75 °C, indicating that the potential stresses due to thermal variations are significantly reduced in the horizontal plane of the part [75]. This, in conjunction with the orthotropic nature of parts made by additive manufacturing shows why the attention of designers of parts must be focused on the stresses in the vertical plane of the part..

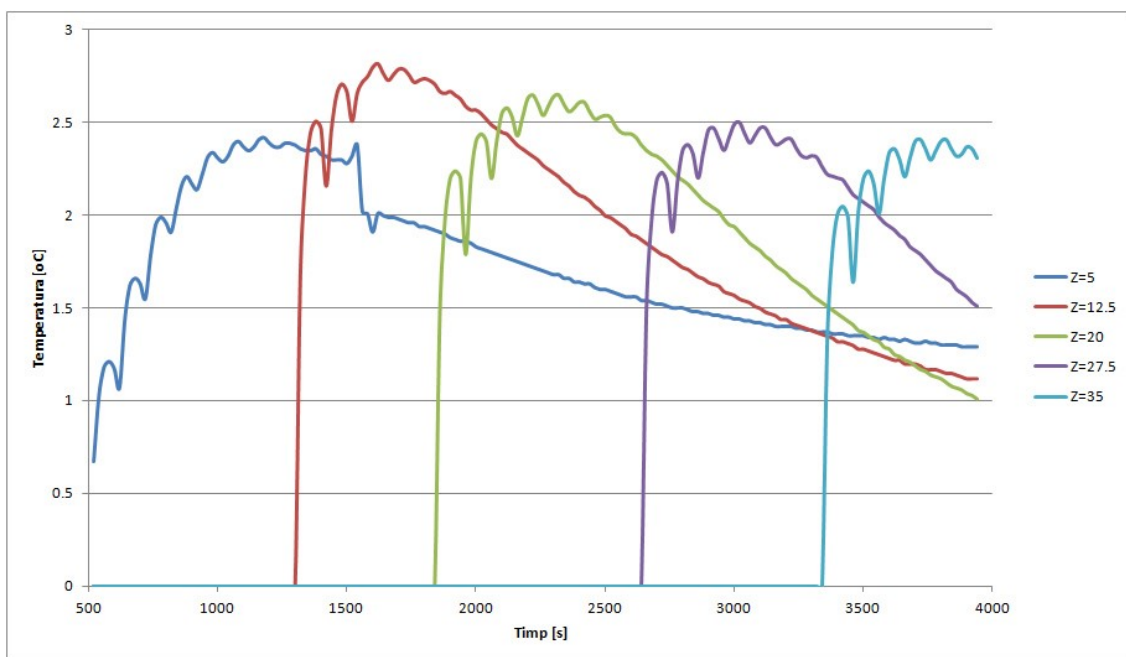


Fig. 6.29. Temperature differences between two points in the same horizontal plane (PLA, 210 °C)

The graph in Fig. 6.30 shows the thermal evolution of the test pieces made of PLA material in case of increase of the deposition temperature from 190 °C to 230 °C. The graphs were drawn for the sensor positioned at a distance $z = 5$ mm from the heated bed.

As the experimental results presented by other works in the field indicate that the fusion of the plastic layers is stronger when the molten filament is deposited at a higher temperature [76], this element represents a potential optimization direction for increasing the mechanical strength of parts manufactured by fused filament fabrication.

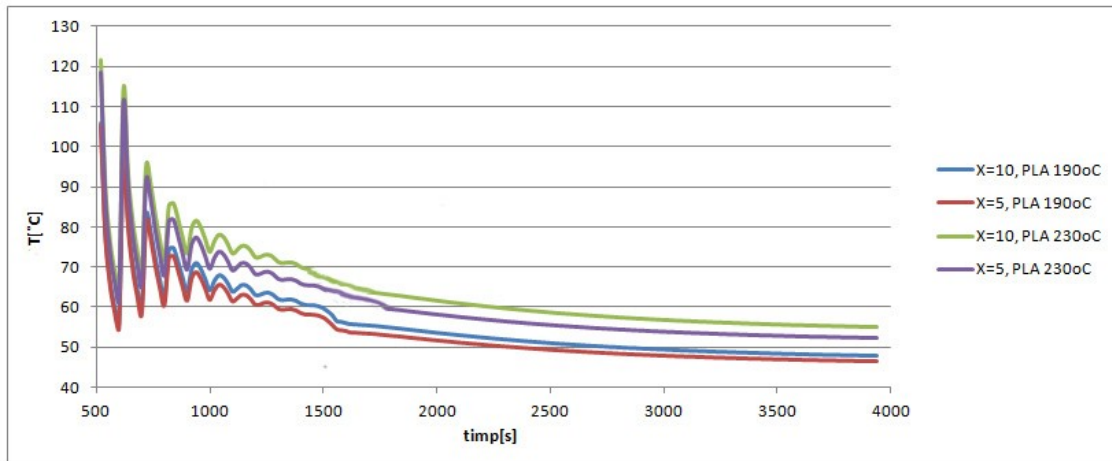


Fig. 6.30. Temperature variation for test parts made of the same material, at different deposition temperatures (PLA, 190°C, 230°C)

When manufacturing a part using a higher filament deposition temperature, it can be seen that the differences between the temperature of the inner volume of the part and that of its surface are higher, which indicates the need to find a solution superior to the heated bed in the case of parts printed at high temperatures (Fig. 6.31).

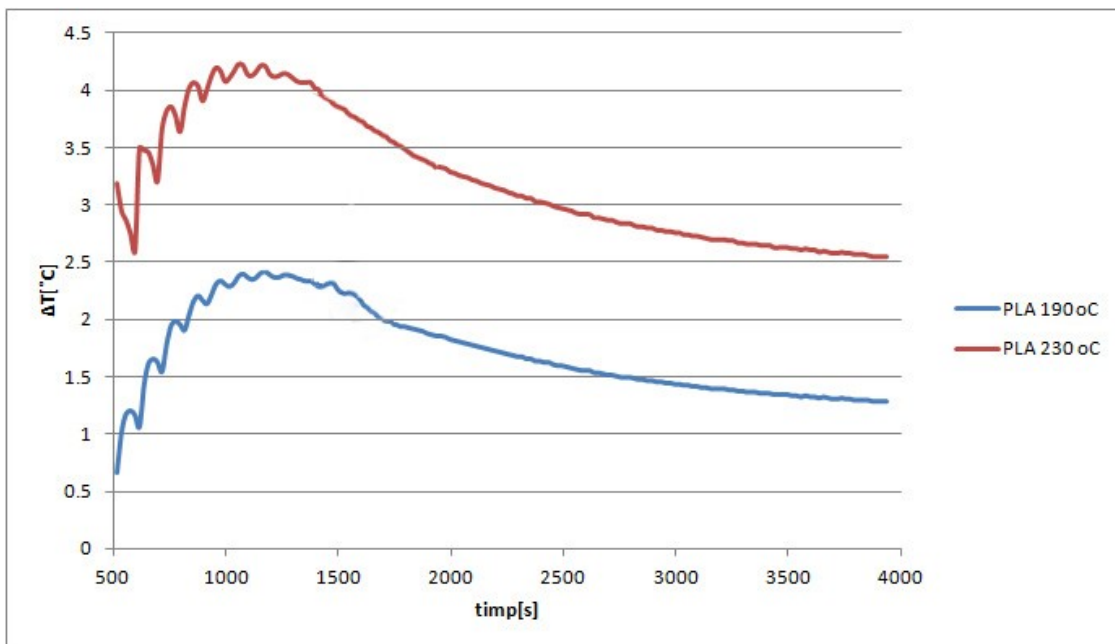


Fig. 6.31. Temperature differences between two points in the horizontal plane (PLA 190 °C, 230 °C)

In order to determine the influence of the heated bed on the manufactured part, experimental measurements were performed in the case of the test parts made from ABS material, with a deposition temperature of 230 °C and a heated bed temperature of 60 °C. The second set of measurements was performed in a manufacturing process with the bed heated to a temperature of 110 °C. As the results of the finite element analysis suggest that the influence of the heated bed leads to the rapid stabilization of the temperature in the lower layers of the part, in order to highlight the effect of increasing the bed temperature from 60 °C to 110 °C, a graph has been drawn that considers temperature sensors positioned at a distance $z = 12.5$ mm from the heated bed (Fig. 6.33)

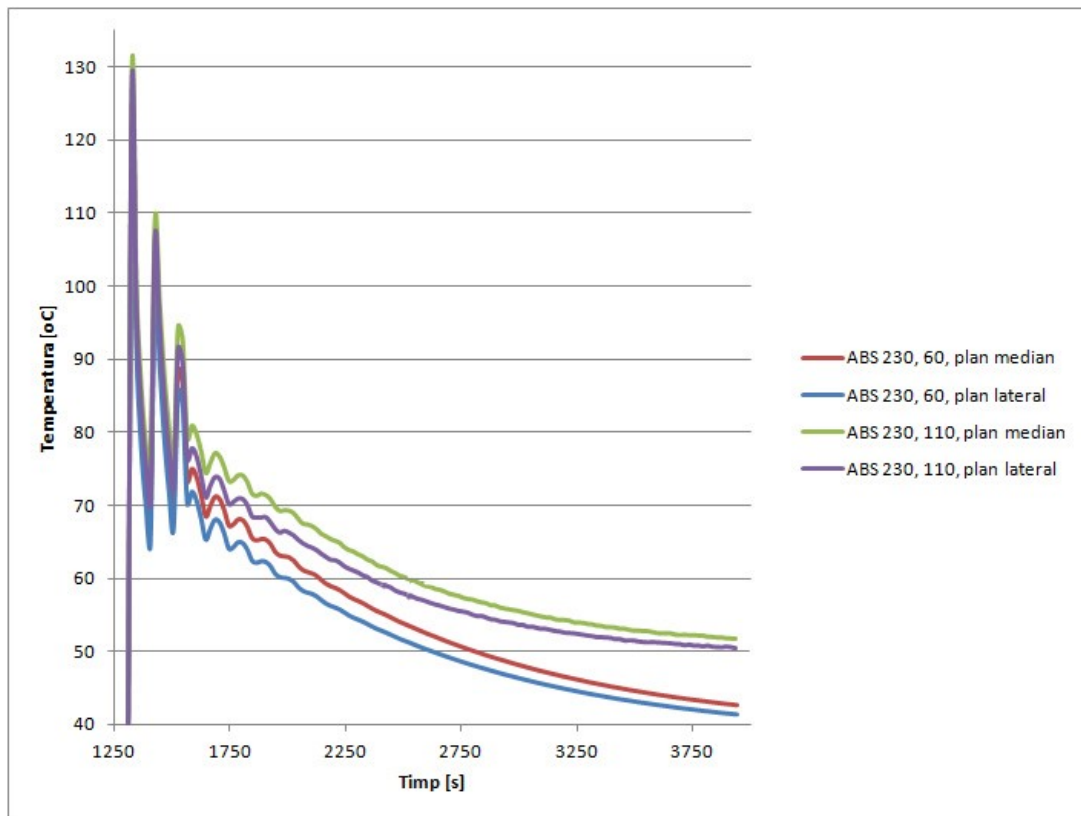


Fig. 6.33. Temperature variation for test parts manufactured using different heated bed temperatures (ABS, bed temperature 60 °C and 110 °C)

The results obtained in this case are as expected, namely, in the case of the bed heated to a higher temperature, the temperature variations are attenuated and the part cools more slowly.

To determine the influence of the chamber temperature on the evolution of the temperature inside the 3D printed part, the experimental measurements made during manufacturing of test parts were compared, initially with the printer chamber open, then closing the chamber and letting the indoor air temperature stabilize around of 45 °C. In both cases, the parts were made of ABS material, with a deposition temperature of 230 °C and a heated bed temperature of 60 °C. The deposition temperature of the material is 230 °C in both cases. Considering the influence of the heated bed previously determined, to visualize the effect of closing the build chamber, a graph of the experimental measurements made by the sensors placed at a distance $z = 20$ mm from the heated bed was drawn (Fig. 6.34).

Another way to experimentally validate the finite element analysis method is to visualize a printing process through a thermography camera. For this purpose, a specimen of dimensions length = 30 mm, width = 5 mm and height = 30 mm was printed on a Zortrax M200 3D printer from a mixture of polycarbonate with ABS. The extrusion temperature was 260 °C. The manufacturing process was recorded with a ThermoCAM SC640 thermal camera (FLIR Systems - Wilsonville, OR, USA). Figure 6.35 shows frame captures in which a temperature distribution similar to that determined by finite element thermal analysis described in this chapter can be observed..

The results of the measurements indicate a much more pronounced impact of the enclosure temperature compared to that of the heated bed temperature.

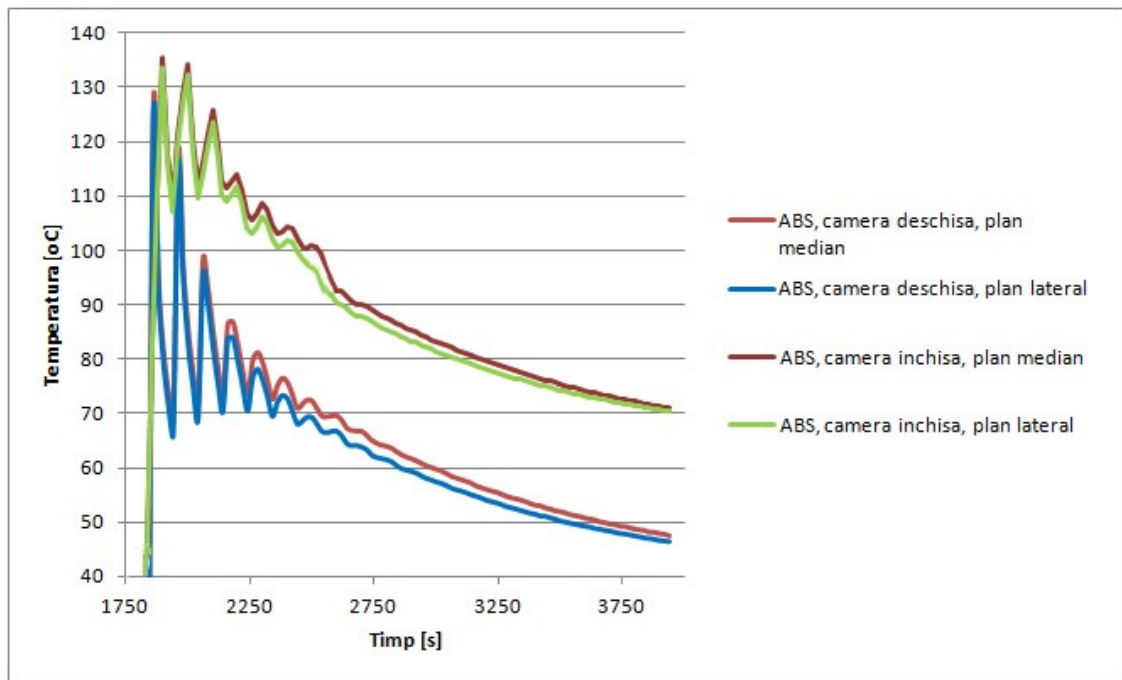


Fig. 6.34. Temperature variation for test parts manufactured using different machine enclosure temperatures (ABS, ambient temperatures 24 °C, 45°C)

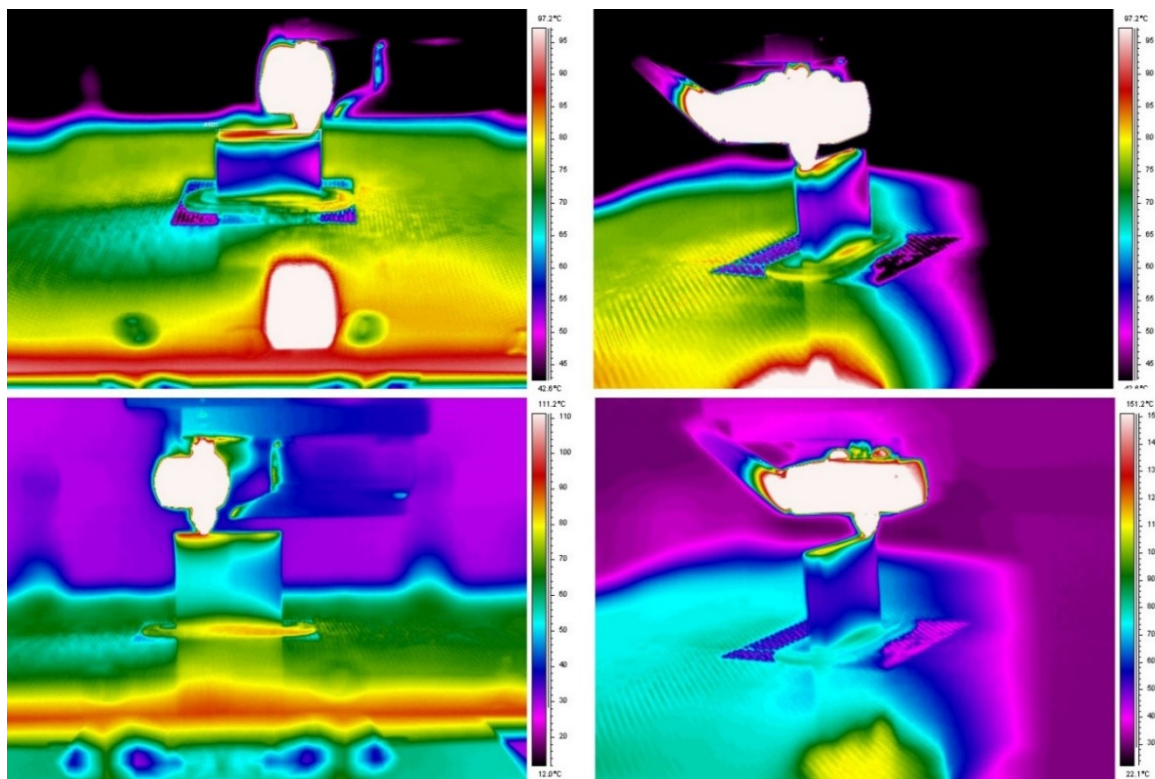


Fig. 6.35. Still frames taken from the ThermoCAM SC640 thermal camera during the additive manufacturing process of a PC + ABS test tube on a Zortrax M200 3D printer

CH. 7 FDM 3D PRINTER WITH A VACUUM BUILD CHAMBER

Previously, it was experimentally determined that the influence of the printer enclosure temperature on the part temperature is much more significant (Fig. 6.34) than the influence of the heated platform, which has a limited effect (Fig. 6.33). These observations are of major importance, given that the objective of doctoral studies is to carry out an additive manufacturing process of objects using special plastics, with high melting temperatures, which requires a system of maintaining the temperature of the parts at adequate values during manufacturing process.

One approach to the problem of using thermoplastic materials with high melting temperatures may be to eliminate the cause of inadequate cooling of the deposited material, namely the phenomenon of thermal convection [77]. This would be possible by depositing molten filament in a vacuum chamber. This approach presents some technical hurdles that need to be overcome:

- Obtaining a vacuum level in the room suitable for the application;
- Development of a motion transmission system that can operate in a vacuum for periods of time specific to the manufacturing process (over 24 hours of continuous operation without outside intervention)
- Transmission of electricity for internal electrical and electronic components;
- Thermal management of components.

Before making a detailed analysis of these issues, a few remarks can be made:

- Vacuum systems for vacuum sublimation plating are widely used in industry; they use high intensity electricity
- The actuators (stepper motors) of special construction can be placed in a vacuum; an alternative is to place them outside the vacuum enclosure and create a system for transmitting motion through the enclosure wall;
- The aerospace industry is an important source of documentation and experimental results for materials and systems used in vacuum.

7.2. THERMAL TRANSFER IN A VACUUM

Heat can propagate through 3 mechanisms:

- Thermal convection - a form of heat transfer specific to fluids (gases and liquids) that depends on the presence of a material that comes into contact with the volume of fluid. Convection is conditioned by the existence of the movement of fluid particles and can be of two types: natural convection, if the fluid particles are moving due to pressure differences generated by temperature, or forced convection, if this movement is produced by external forces (generated by pumps, fan, etc.).
- Thermal conduction - is the propagation of temperature through the volume of a material by collisions between elementary particles that are part of the material.
- Thermal radiation - is the phenomenon by which condensed bodies emit electromagnetic radiation.

7.2.1 Heat transfer in the case of the extruder of a machine for additive manufacturing by fused filament fabrication.

By eliminating the phenomenon of thermal convection, the temperature transfer in vacuum is done predominantly by thermal conductivity. In the case of an additive manufacturing process by deposition of topical filament, two distinct moments can be identified related to this aspect, namely:

- Thermal conductivity and heat transfer from the heated head to the filament and to the extruder structure when the thermoplastic filament melts;

- Thermal conductivity and heat transfer from the volume of extruded material in the machine platform.

In the case of the extruder, the heat transfer occurs through the thermal tube and through the material contained in it (Fig. 7.6).

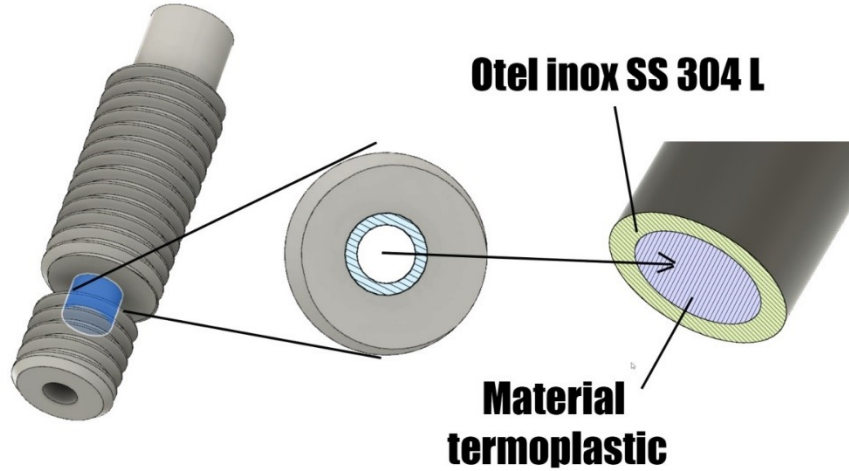


Fig. 7.6. Heatbreak and its section

In the section with the thinnest walls, heatbreak has an inner diameter of 2 mm and an outer diameter of 2.8 mm, resulting in a section area of 3,016 mm². During operation, the narrow part of this tube is filled with thermoplastic material at a temperature close to the extrusion temperature. Therefore, the cross-sectional area of the thermoplastic material is 3.14 mm².

Thermal transfer through conductivity can be expressed by Fourier's law (Fig. 7.7):

$$q_x = kA \frac{dT}{dx}, \quad (7.17)$$

where

q_x – the amount of heat transferred [W, J/s];

k – the thermal conductivity coefficient of the material [W/mK];

A – material cross-section area [m²];

dT – temperature difference [K];

dx – material thickness [m].

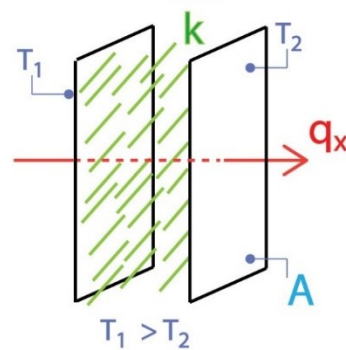


Fig. 7.7. Heat transfer by thermal conduction

7.2.2 Heat transfer in the case of deposited material

The amount of heat transferred by the deposited material depends on the volume of extruded material, the extrusion speed and the specific heat of the material. The specific heat (material constant) is determined from the relationship:

$$Q = cm\Delta T, \quad (7.18)$$

where

Q is the amount of heat,

c – specific heat (material characteristic),

m – material mass,

ΔT – temperature difference.

The amount of heat Q that must be released by the thermoplastic material after deposition (Table 7.7) for the part to reach the appropriate temperature is calculated using the relation:

$$Q = c \cdot \rho \cdot 10^{-3} \cdot R_{dep} \cdot \Delta T, \tag{7.19}$$

where

c – specific heat [J/g·K]; ρ – density g/cm³; R_{dep} – material deposition rate [mm³/s]; ΔT – temperature difference.

Table 7.7. The heat ceded by the thermoplastic material after deposition

Material	Specific heat [J/gK]	Extrusion temperature [°C]	Part temperature [°C]	Density [g/mm ³]	ΔT [°C]	Q min [W]	Q max [W]
PC	1.41	280	80	0.00122	200	0.069	2.064
PEI	1.10	315	95	0.00127	220	0.061	1.844
PPS	0.95	350	105	0.00134	235	0.060	1.795
PEEK	0.32	400	120	0.00132	280	0.024	0.710

7.3 VACUUM BUILD CHAMBER 3D PRINTER DESIGN

7.3.1 Dimensioning the resistance structure for the sealed chamber

It is recommended that the walls of a vacuum chamber be made of metal or non-metal alloys. Due to its good strength, machinability and weldability characteristics, the manufacture of aluminum alloy walls EN-AW-5083 with the chemical composition AlMg4,5Mn0,7 was chosen..

To dimension the thickness of the camera walls, a finite element analysis was performed using the simulation module integrated in the Autodesk Fusion 360 software. The considered model is a square plate measuring 340 × 340 mm with standardized thicknesses of 5, 6, 8 , 10 mm. The material assigned to the model was taken from the application database and is “Aluminum 5083 87 cold formed” with a breaking strength of 270 MPa. The gravitational force and a pressure of 1.2 bar were applied to the front surface of the plate, equivalent to the pressure difference between the pressure in the vacuum chamber and the atmospheric pressure, with a safety factor of 1.2. The volume of the virtual model was processed with a tetrahedral structure mesh with a maximum element size of 1% of the model dimensions

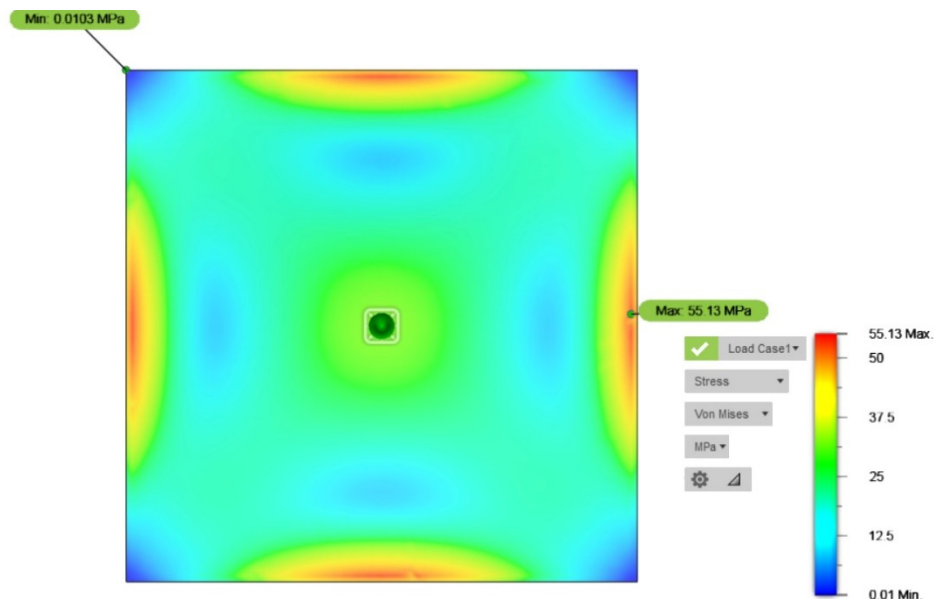


Fig. 7.9. The result of the analysis with finite elements - Tensions appearing in the 8 mm thick plate

As it can be seen in Fig. 7.9, the maximum stress in the material for a plate thickness of 8 mm is 55.13 MPa, below one third of the allowable stress of 150 MPa at which the material begins to deform plastically. According to the results, the thickness of the material of more than 5 mm is sufficient to withstand the forces to which it is subjected during use. The maximum elastic deformation of the material is between 0.3307 and 2.6210 mm. Table 7.8 presents the results of the finite element analysis for standardized plate thicknesses.

Table 7.8. The results of the finite element analysis - predimensioning of plates from Al 5083

Thickness [mm]	Tensile load [MPa]	Max deformation [mm]
10	34,15	0.3307
8	55.13	0.6431
6	97.89	1.5190
5	142	2.6210

7.3.2 Producing the relative motion of the extruder in relation to the machine platform

When constructing the mechanism that produces the relative motion of the extruder relative to the platform surface, the constructive variants of 3D printers presented in Chapter 3 were taken into account..

The first considered criterion is the volume occupied by the mechanical structure of the movement system. The working space of the machine must be large enough to allow the manufacture of standard ASTM D638 samples used in destructive testing. A workspace of 180 x 180 x 180 mm was thus established. The volume occupied by the mechanical structure must be minimal, in order to reduce the loads acting on the walls of the enclosure due to the pressure difference. To meet this criterion, the platform was fixed in the horizontal plane and the relative movement of the extruder in this plane is performed by a double portal type system. The relative movement in the vertical plane is achieved by translating the platform on the vertical axis.

A second criterion is the positioning of the stepper motors outside the vacuum enclosure and the transmission of the rotational motion through the enclosure wall. This is made possible by the drive and transmission system represented in Figs. 7.12.

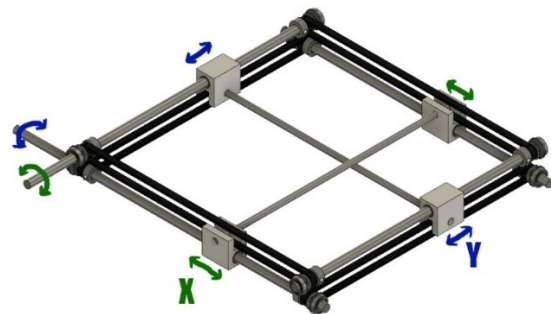


Fig. 7.12. Motion transmission system - XY horizontal axes of motion

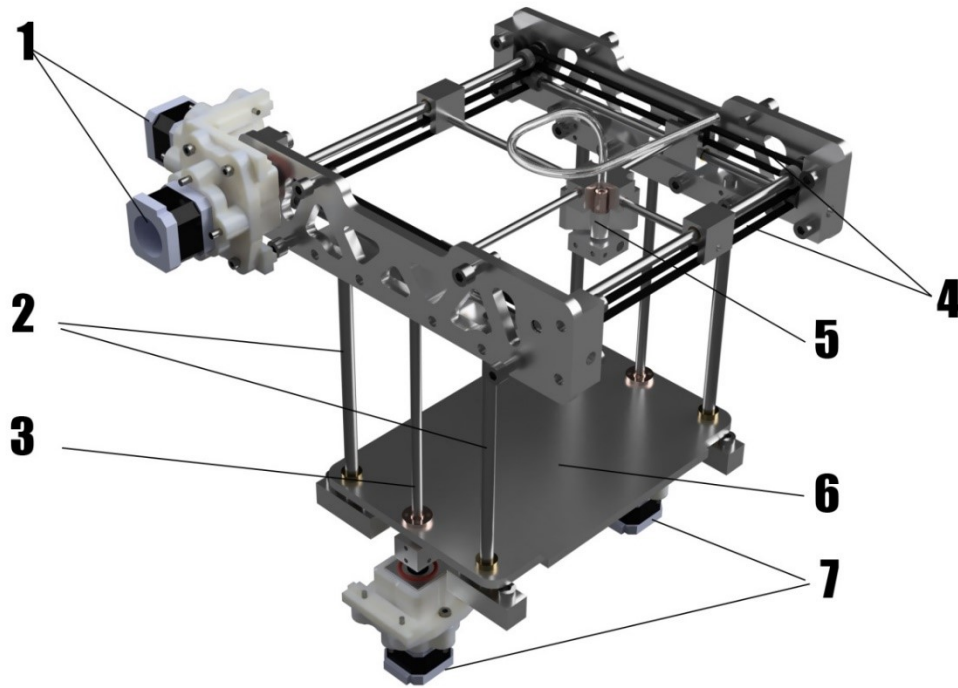


Fig. 7.13. Motion axes structure

The stepper motors (Fig. 7.13 - 1) located outside the enclosure, transmit the rotational motion through the enclosure wall. The rotational motion is transformed into translational motion by means of transmission belts (Fig. 7.13 - 4). The two stepper motors are positioned on perpendicular axes, producing the motion of the extruder (Fig. 7.13 - 5) in the XY horizontal plane. The printing platform (Fig. 7.13 - 6) moves on the vertical axis Z, being driven by stepper motors (Fig. 7.13 - 7) that rotate the trapezoidal screw (Fig. 7.13 - 3). Guiding the vertical axis is done using guide axes (Fig. 7.13 - 2).

7.3.3 Linear axes actuation

The linear shaft drive assembly is one of the complex elements of the system, as it must drive the linear shafts from outside the vacuum enclosure. The transmission of the rotational motion through the stainless steel shaft (Fig. 7.14-1) is done through the walls of the vacuum chamber. For this reason, the drive system includes sealing elements. The sealing of the rotating shaft is done with a seal made of fluoropolymer material (Fig. 7.14-4) with low coefficient of friction and wear resistance. The oil seal is prestressed in the housing (Fig. 7.14-5) using a stainless steel outer ring. The oil seal is optimized for vacuum applications, with prestressing on the inner shaft by means of an elliptical spring. In order to meet the concentricity requirements necessary for sealing, the stainless steel shaft is guided by radial ball bearings located both in the vacuum part (Fig. 7.14-2) and in the part subjected to atmospheric pressure (Fig. 7.14-6). In order to reduce wear and improve sealing, low degassing vaseline is introduced between the oil seal and the bearing. The housing that contains the sealing components is inserted into the housing of the assembly (Fig. 7.14-7) and attached to the wall of the printer with fasteners (7.14-8). A viton frontal o-ring (Fig. 7.14-3) seals the system. The rotational motion is transmitted from the stepper motor (Fig. 7.14-11) to the shaft by means of a flexible coupling (Fig. 7.14-10) which has the role of reducing vibrations and compensating for the eccentricity of the two coupled shafts.

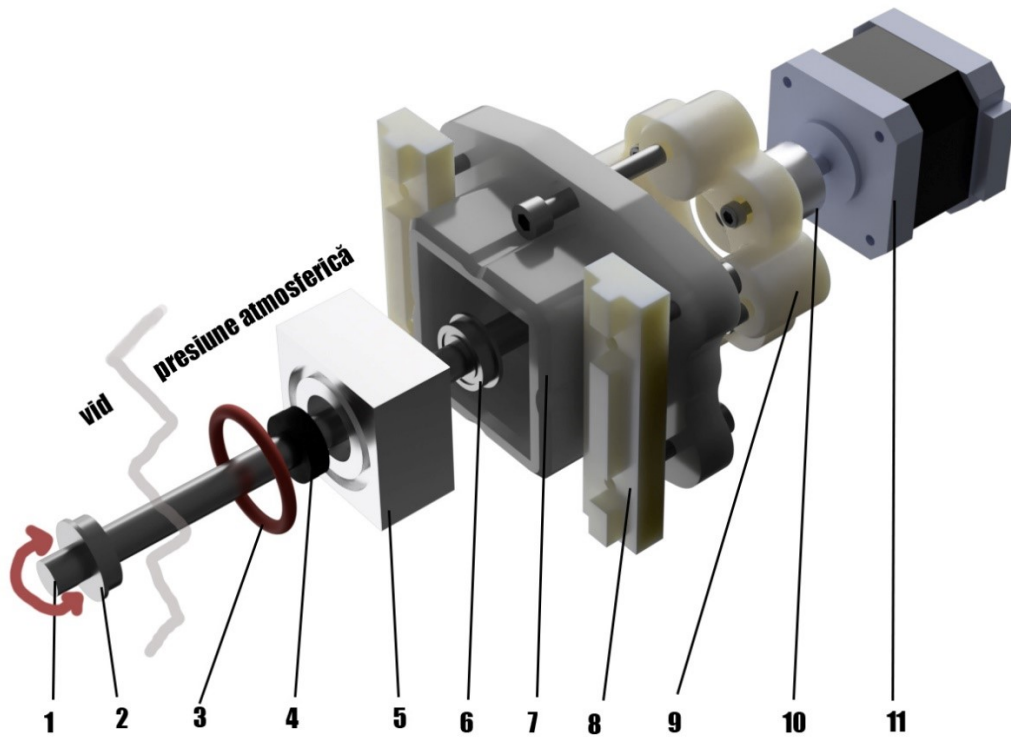


Fig. 7.14. Linear axes actuation assembly

7.3.4 Thermoplastic filament extruder

Chapter 6 presented finite element thermal analyses for two types of extruders used in commercially available 3D printers. The recommendations made after analyzing the results of these simulations were applied to the design of an extruder (Fig. 7.15) capable of processing thermoplastic filament at high temperatures and sub-atmospheric pressure.

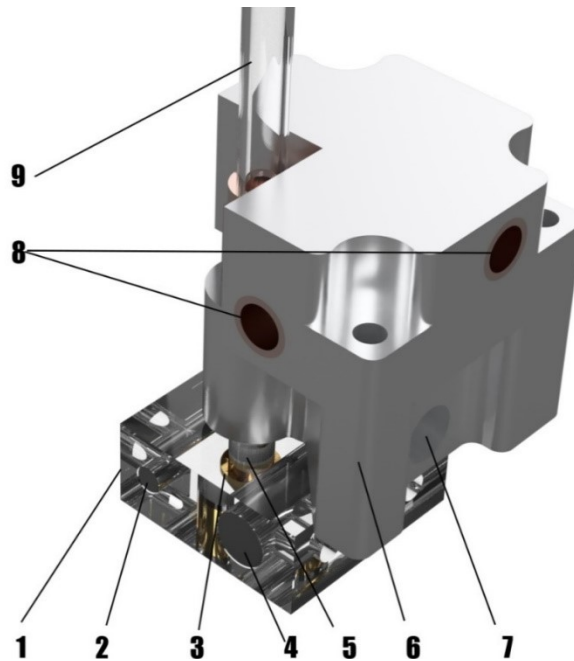


Fig. 7.15. Extruder assembly

According to the recommendations, the brass extrusion nozzle found in commercially available extruders has been replaced with a stainless steel extrusion nozzle (Fig. 7.15-3) which

maintains its mechanical properties at temperatures of 400 °C. Also, the tube for slowing down the heat transfer made of teflon was removed and the filament is guided through a stainless steel tube (Fig. 7.15-5). The heating of the extrusion nozzle and the melting of the thermoplastic material is done by a ceramic heater with a power of 80 W (Fig. 7.15-4). The temperature is monitored with a PT100 type temperature sensor usable up to temperatures of 500 °C (Fig. 7.15-2). The sensor, the ceramic cartridge and the extrusion nozzle are fixed in an aluminum heating block (Fig. 7.15-1).

As the air in the enclosure is evacuated, the extruder body (Fig. 7.15-6) is cooled using liquid cooling (Fig. 7.15-7). Keeping the extruder body at temperatures below 60 °C is done to prevent heat transfer by conduction to other parts of the machine and to keep the guide bushes for translating the extruder horizontally (Fig. 7.15-8) at appropriate temperatures..

7.3.5 Passing electric current through the vacuum chamber walls

3D printers for fused filament fabrication require some electrical components to be positioned inside the enclosure (end-of-travel sensors, ceramic heater cartridge, temperature sensors, etc.). Therefore, in the case of a vacuum chamber, it is necessary to pass the electrical conductors that supply these components through the wall of the vacuum chamber, without compromising the vacuum level inside.

The choice of sealing materials and the dimensioning of the feedthrough elements (Fig. 7.16) will be made taking into account the intensity and type of current required.:

- 220 VAC, 0.5 A for the ceramic heating cartridge;
- 5 VDC, 300 mA for temperatre sensors;
- 3.3 VDC for end-of-travel sensors;

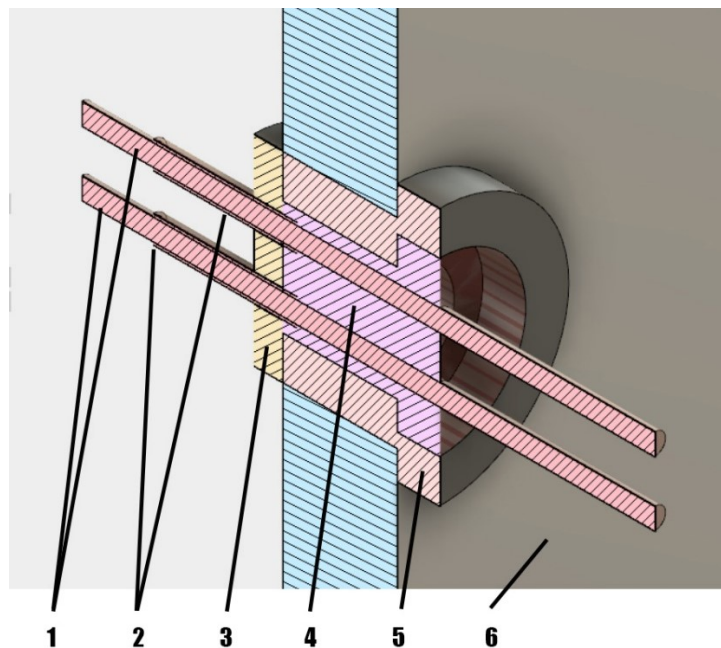


Fig. 7.16. Feedthrough assembly for electrical conductors

The electrical conductors (Fig. 7.16-1) are sealed using a volume of epoxy resin (Fig. 7.16-4) with degassing properties suitable for use in vacuum. To limit the mass of resin lost by evaporation, its surface that is exposed to the vacuum environment is covered with a stainless steel lid (Fig. 7.16-3). The conductors are electrically insulated in the lid area using kapton tape (Fig. 7.16-2). The volume of epoxy resin is obtained by casting the resin in an aluminum connector (Fig. 7.16-5). The connector is fixed to the wall of the vacuum chamber (Fig. 7.16-

6) by screwing. The diameter of the connector and the volume of resin required for sealing will be dimensioned according to the number of electrical wires.

7.4 WORKING PRINCIPLE

Within the doctoral program, research was carried out on the additive manufacture of special plastic parts (with high melting temperatures) that require a system to maintain the temperature of the parts at adequate values during the manufacturing process to prevent defects caused by internal thermal stresses.

Research in the field on parts made of ABS and polyamides in an inert nitrogen medium [85] shows that the mechanical properties of printed parts are better in the absence of oxygen.

The application chosen for detailed investigation is the manufacture of parts in the absence of oxygen, in a vacuum chamber. The exclusion of air aims to standardize the heat transfer process of the 3D printed part during manufacturing, in order to reduce the influence of repeated cooling / heating cycles on the mechanical properties of the part.

In a system, heat can propagate through 3 mechanisms:

- Thermal convection - a form of heat transfer specific to fluids (gases and liquids) that depends on the presence of a material that comes into contact with the volume of fluid. Convection is conditioned by the existence of the movement of fluid particles and can be of two types: natural convection, if the fluid particles are moving due to pressure differences generated by temperature, or forced convection, if this movement is produced by external forces (generated by pumps, fan, etc.).
- Thermal conduction - is the propagation of temperature through the volume of a material by collisions between elementary particles that are part of the material.
- Thermal radiation - is the phenomenon by which condensed bodies emit electromagnetic radiation.

As the atmospheric air in the vacuum chambers, which is the convection heat propagation medium, is evacuated, the phenomenon of convection heat transfer is gradually eliminated. What determines whether the heat transfer by convection takes place, as well as the amount of heat transferred, is the average free flow of air molecules in the vacuum chamber. The average free path is the average distance traveled by a molecule inside a volume until it collides with another molecule. In the kinetic theory of gases their properties are explained on the basis of the movements of molecules. In this theory, gas molecules move freely, continuously, depending on temperature, influencing each other only at the moment of collision.

In support of the research, a prototype of a 3D printer with a vacuum chamber was made, with the help of which a series of parts printed both in vacuum and in the atmosphere at room temperature were manufactured. The parts were subjected to mechanical tests to determine their tensile strength.

7.5 MECHANICAL STRUCTURE

The vacuum chamber is made of 5083 aluminum sheet with a thickness of 8 mm processed by water jet cutting, with interlocking geometry for easier assembly. The gaps between the walls were sealed using epoxy resin. The vacuum chamber is mounted on an external structure of industrial aluminum profiles. The stepper motors that drive the printer's motion system are mounted on the same outer structure.

The printing bed is made of EN-AW-5083 aluminum alloy plate with a thickness of 8 mm and has a perforated plate made of FR4 material on the surface. The role of the perforated plate is to retain the auxiliary raft structure on which the part is made, preventing its delamination during printing. The platform moves on the vertical axis Z (Fig. 7.17), the movement system consisting of two stepper motors, rigidly coupled to a trapezoidal screw with

2 starts and 8 mm pitch. The platform is guided at each end on two linear guides. The guide bushes and the movement nut are made of sintered bronze.

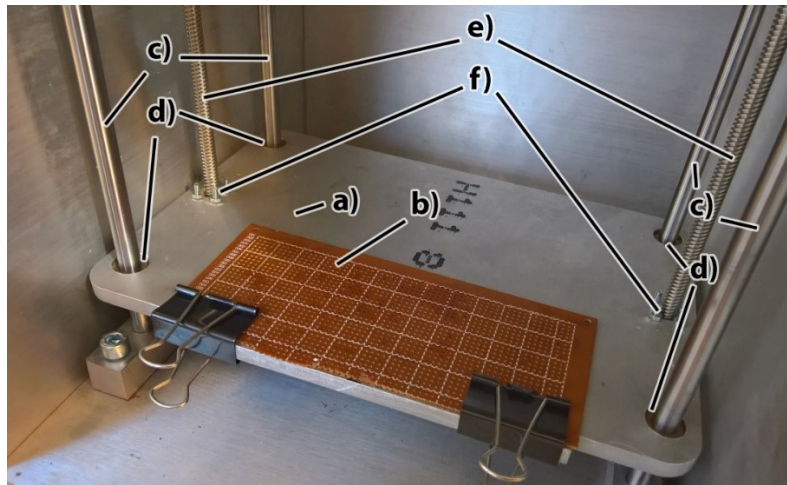


Fig. 7.17. Printing platform and vertical axis Z: a) platform; b) perforated plate; c) linear guide axes; d) guide bushes; e) trapezoidal movement screws; f) movement nuts.

The horizontal axes X and Y (Fig. 7.18) are actuated by means of a mechanism with a 6 mm wide rubber drive belt, reinforced with Kevlar wires. Bronze bushes allow the extruder to slide freely on the stainless steel guide shafts..



Fig. 7.18. Horizontal axes of the 3D printer.

For mechanical actuation, the motion must be transmitted through the wall of the vacuum chamber without losing the vacuum inside. For this purpose, a sealing system (Fig. 7.19) with a viton seal with elliptical prestressing spring for vacuum sealing applications is used. The oil seal is inserted into an aluminum housing that attaches to the wall of the vacuum chamber through a flat seal with an o-ring seal. The shaft that rotates to drive the belt wheel and engage the drive belt is connected to the stepper motor shaft through an aluminum elastic coupling.

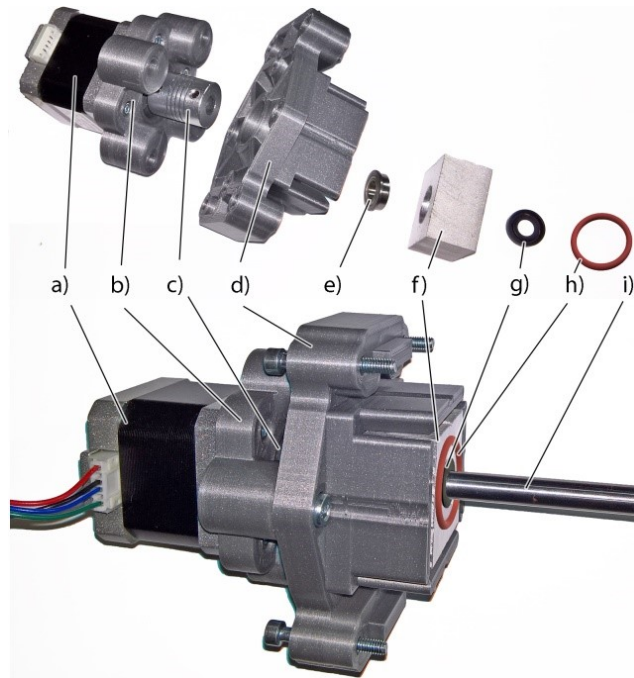


Fig. 7.19. Shaft sealing system for motion transmission. a) stepper motor; b) intermediate motor support (3D PLA print); c) elastic coupling; d) motor support (3D PLA printing); e) flange bearing f) bearing and energised seal housing; g) energised seal; h) o-ring; i) rotation shaft.

7.6 ELECTRICAL AND ELECTRONIC COMPONENTS

The heaters and the components whose role is to control the printing temperature, as well as the vacuum pump, are supplied from a mains socket, with 230 VAC. The rest of the printer components are powered by a 12 V, 20 A (240 W) DC power supply

Ceramic resistor - a resistor with a power of 80 W that works at 230 VAC is used. With a power twice the that of heating cartridges commonly found in commercially available printers (30–40 W), the possible printing temperature is 400 °C.

Water pump - to cool the heated end of the extruder it is necessary to use a water cooling circuit powered by a 12 VDC pump.

The vacuum pump is a two-stage pump with a maximum vacuum of 0.2 Pa (2×10^{-3} mbar). The technical characteristics of the vacuum pump can be found in Table 7.13.

Table 7.13. Technical characteristics of the vacuum pump

Characteristic	Value
Air flow	51 L /min
Vacuum	2×10^{-1} Pa (1.5×10^{-3} Torr)
Power	250 W
Inlet	1/4" SAE
Oil capacity	200 ml
Weight	9 kg

The printer functions are controlled by a RAMPS 1.4 expansion board attached to an Arduino MEGA 2560 microcontroller. The expansion board includes 5 drivers for stepper motors type Allegro A4988 [86].

The extrusion temperature is adjusted separately from the main controller, by means of a circuit (Fig. 7.22) consisting of a PID temperature controller type REX-C100 with temperature monitoring interval between 0 °C and 999 °C which receives a signal from a K-type thermocouple and switches a ceramic resistor through a solid-state type relay. This solution was

chosen due to the limited interface of the RAMPS 1.4 expansion board that allows only the interface with NTC type sensors, in which case the maximum monitored temperature can be up to 250 °C

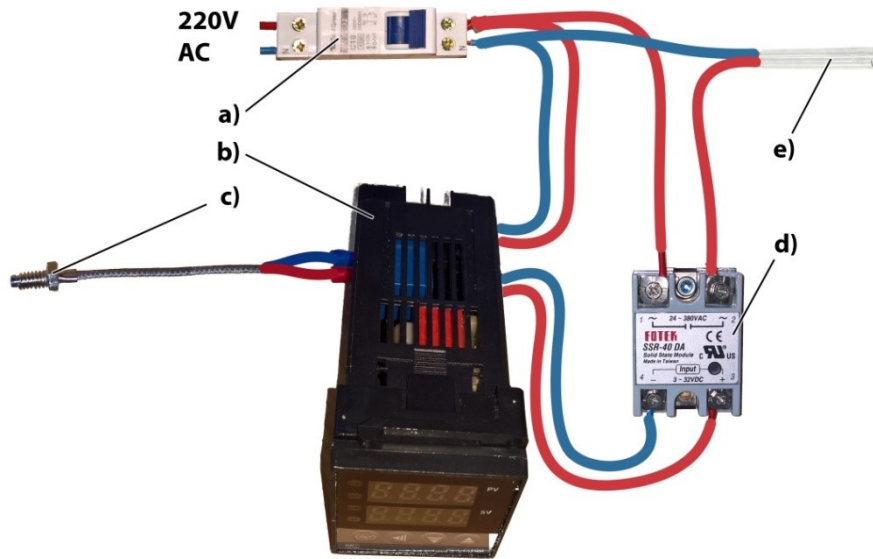


Fig. 7.22. Extrusion temperature control circuit. a) circuit breaker; b) Temperature controller REX-C100; c) thermocouple type K; d) solid state relay; e) ceramic resistance

Stepper motors. The printer motion axes and the filament supply system are driven by stepper motors type NEMA17 model 42BYGHW609 with 1.8° rotational pitch. These are controlled by Allegro A4988 stepper motor drivers (2A max) in a 1/256 microstepping configuration.

7.7 SOFTWARE AND FIRMWARE

7.7.1 Firmware

The Marlin 1.3 open-source firmware [87] is loaded on an Arduino MEGA 2560 controller, which has been adapted to the application-specific mechanical and process characteristics. Because the temperature is not directly controlled by the microcontroller and is set separately in the REX-C100 temperature controller, the minimum extrusion temperature (standard - 170 °C) has been deactivated. Similarly, the thermal protection function has been deactivated. This would turn off the power supply if the temperature sensor does not detect the temperature rise with the power supply. Marlin 1.3 firmware comes preconfigured for Allegro A4988 stepper motor drivers.

7.7.2 Slicer

The printer has been configured in the Simplify 3D 4.0 slicer program (Ohio, USA). A series of instructions are executed at the beginning of each printing program. The extruder is brought to the zero position, the platform on the Z axis is recalibrated and the extruder is purged. At the end of the printing program, another series of instructions is executed that bring the extruder and the platform back to zero and signal the end of the program.

CH. 8. EXPERIMENTAL TESTING AND RESULTS

8.1 METHOD AND MATERIALS

Two materials were selected for testing the device and the manufacturing method: ASA (acrylonitrile styrene acrylate) and PEI (polyetherimide).

ASA - acrylonitrile acrylate styrene or styrene acrylonitrile acrylic is a thermoplastic material produced as an alternative to ABS (acrylonitrile butadiene styrene) and is widely used in the automotive industry. Structurally, ASA is very similar to ABS but is more resistant to weather and ultraviolet radiation, more resistant to long-term high temperatures and more resistant to alcohols and cleaning agents. ASA retains its gloss, color and mechanical properties when exposed to the open air. It has good chemical and thermal resistance, high gloss, good antistatic properties and is hard and rigid. It is used in applications that require weather resistance, such as commercial displays, vehicle exterior or outdoor furniture.

ASA filament with a diameter of Ø1.75 mm was sourced commercially, sold under the ApolloX brand (Formfutura - Nijmegen, the Netherlands).

PEI - polyetherimide is a thermoplastic material with a high melting point, used especially in food, chemical and medical instruments due to its chemical stability, resistance to solvents and fire and due to the possibilities of sterilization. Ultem is a family of polyetherimides created in the early 1980s by Joseph G. Wirth. Ultem 1000 (standard resin, without additives) has high dielectric strength, does not burn and emits very little smoke. Ultem products can be processed by cutting, have very good mechanical properties (strength, rigidity) and can be used continuously at temperatures up to 170 °C.

PEI filament with a diameter of Ø1.75 mm was purchased from the market, sold under the Thermax brand (3DXTech - Grand Rapids, MI, USA). The resin from which the filament was made is sold under the brand Ultem 1010 (SABIC - Riyadh, Saudi Arabia).

The dimensions of the test specimens were chosen based on the standard for testing ASTM D638 type I plastics [88] and their minimum section is 3.5 x 13 mm.

The manufacturers' recommendations were taken into account when setting the extrusion temperatures. A total of 12 specimens were manufactured, three for each material and conditions of the printing environment (atmosphere / vacuum). The specimens were manufactured with a material layer thickness of 0.2 mm, with 3 outer contours and 100% infill, alternating between -45° / + 45° the trajectory used to fill the inner volume of the piece. The extrusion temperature was 250 °C for ASA material and 375 °C for PEI.

Due to the large difference between the melting temperatures of the two materials, the stainless steel extrusion nozzle was replaced after changing the material. All specimens were manufactured in a horizontal position.

8.2 SURFACE QUALITY AND DIMENSIONAL ACCURACY

The dimensional accuracy of the specimens made was measured after printing with an electronic caliper and it was found that there are no significant differences in the case of the parts printed in the vacuum chamber compared to those printed in the atmosphere at room temperature. In the case of two of the ULTEM specimens printed in atmospheric conditions, a slight delamination of the part from the shelf-type auxiliary structure was found. All ASA specimens, as well as ULTEM 1010 vacuum-printed specimens showed good adhesion of the layers.

It is presented in the literature that the removal of oxygen, for example using inert gas [89] can lead to improved surface quality of printed parts. The roughness of surfaces can be analyzed using atomic force microscopy..

To compare the quality of the surfaces, the printed parts made of Ultem 1010 material were analyzed using the NTEGRA Probe NanoLaboratory atomic force microscope. The pieces were inspected on the side surface, in order to be able to observe the roughness of the surfaces at the joints between the successively deposited layers of material. The inspection was done along the deposited filaments (Fig. 8.6).

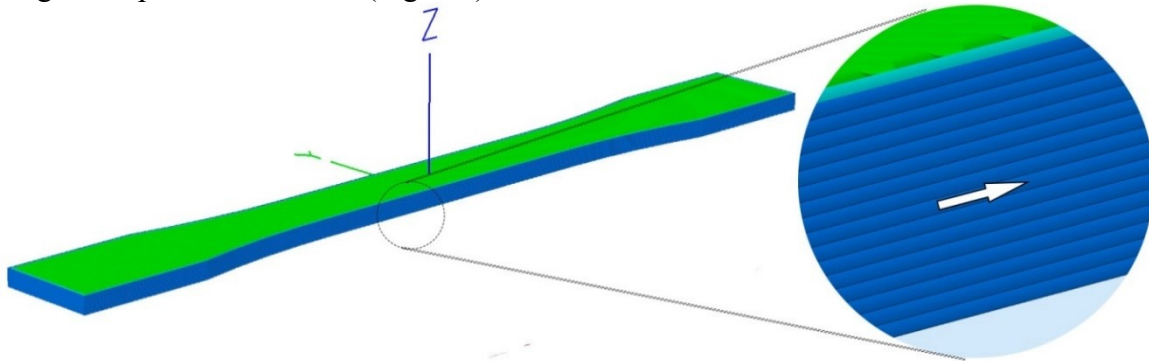


Fig. 8.6. Scanning direction

Using the data taken by the atomic force microscope, three-dimensional graphs (Fig. 8.9, Fig. 8.11) were drawn for the inspected surfaces of the two types of parts. Data on the surface quality of the parts were extracted using the NOVA software and can be found in Table 8.3.

Table 8.3. Surface roughness of 3D printed parts

Printing environment	Roughness Ra [μm]
Atmospheric pressure	6.50 ± 0.26
Low pressure	6.52 ± 0.21

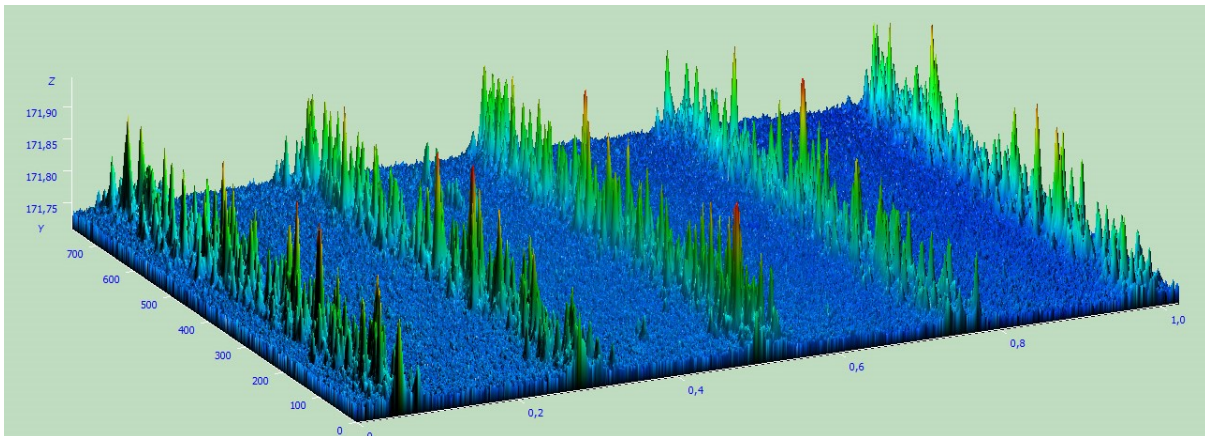


Fig. 8.9. Profile of the side surface of the piece made of Ultem 1010 material printed under atmospheric conditions

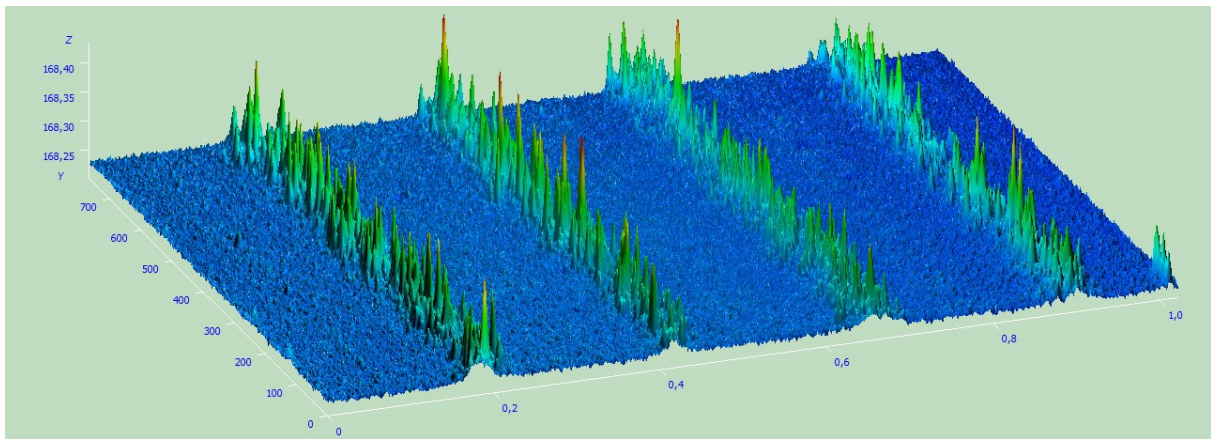


Fig. 8.11. The side surface profile of the Ultem 1010 part printed under low pressure conditions

8.3 TENSILE STRENGTH TESTING

In order to determine the mechanical properties of the parts resulting from vacuum printing, tensile tests were carried out on specimens of the dimensions specified above. The tests were performed on a universal Hounsfield H10KT test machine with a maximum load capacity of 10 kN. The tests were performed with a pretension of 5 N and a loading speed of 5 mm / min, at an ambient temperature of 24 °C and a humidity of 60%

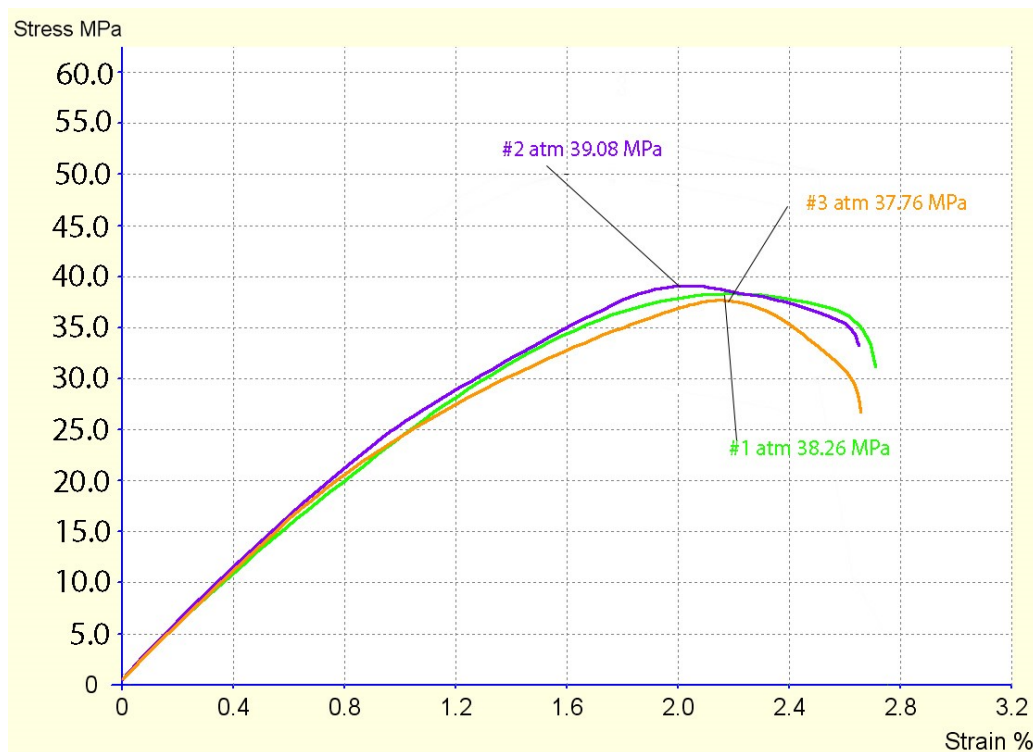


Fig. 8.14. Graph of tensile test results - ASA specimens printed under atmospheric pressure

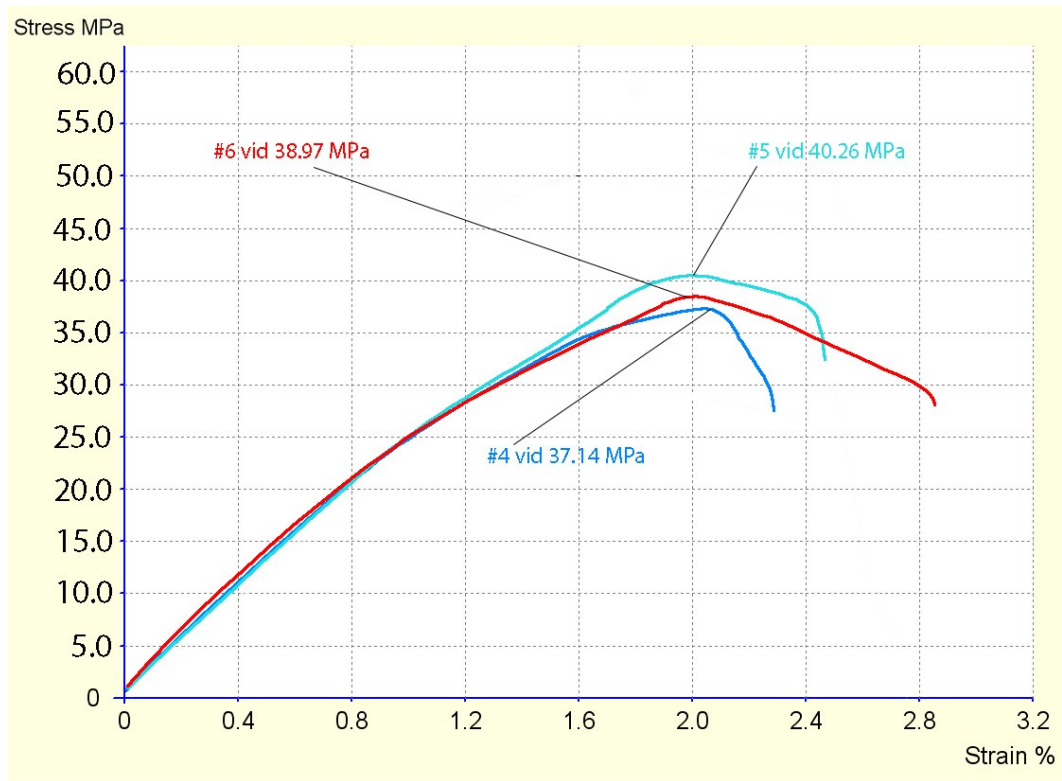


Fig. 8.15. Graph of tensile test results - vacuum-printed ASA specimens

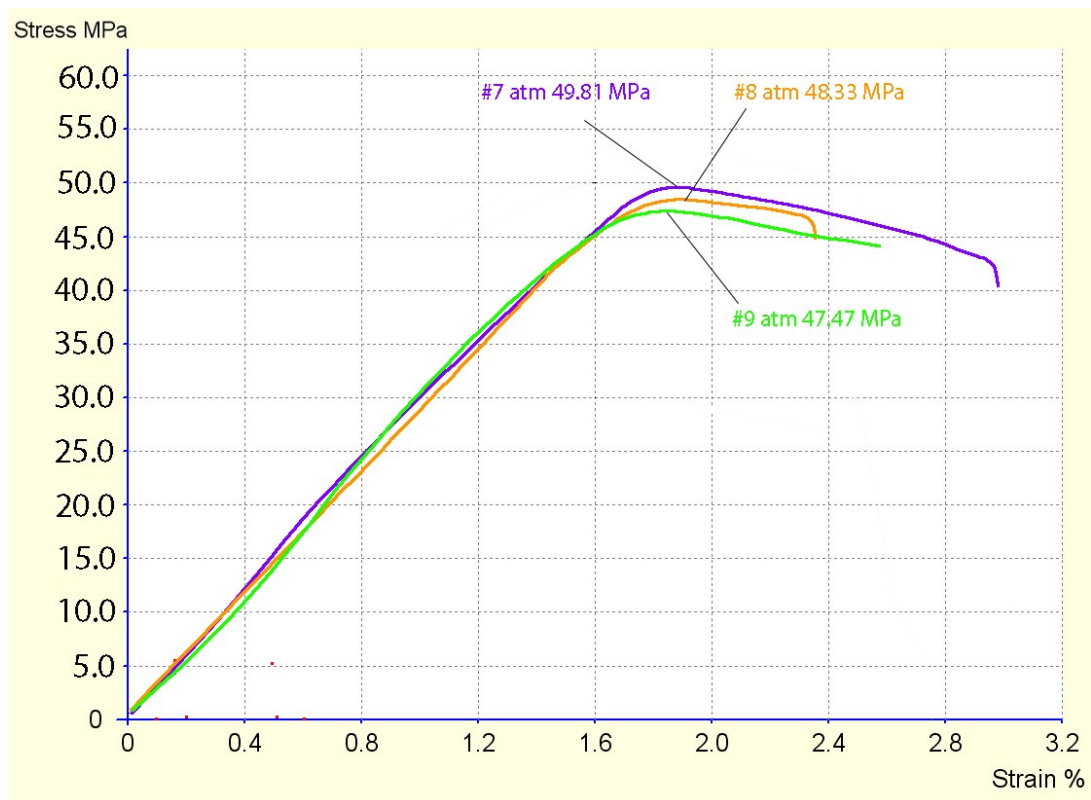


Fig. 8.16. Graph of tensile test results - ULTEM 1010 specimens printed under atmospheric pressure

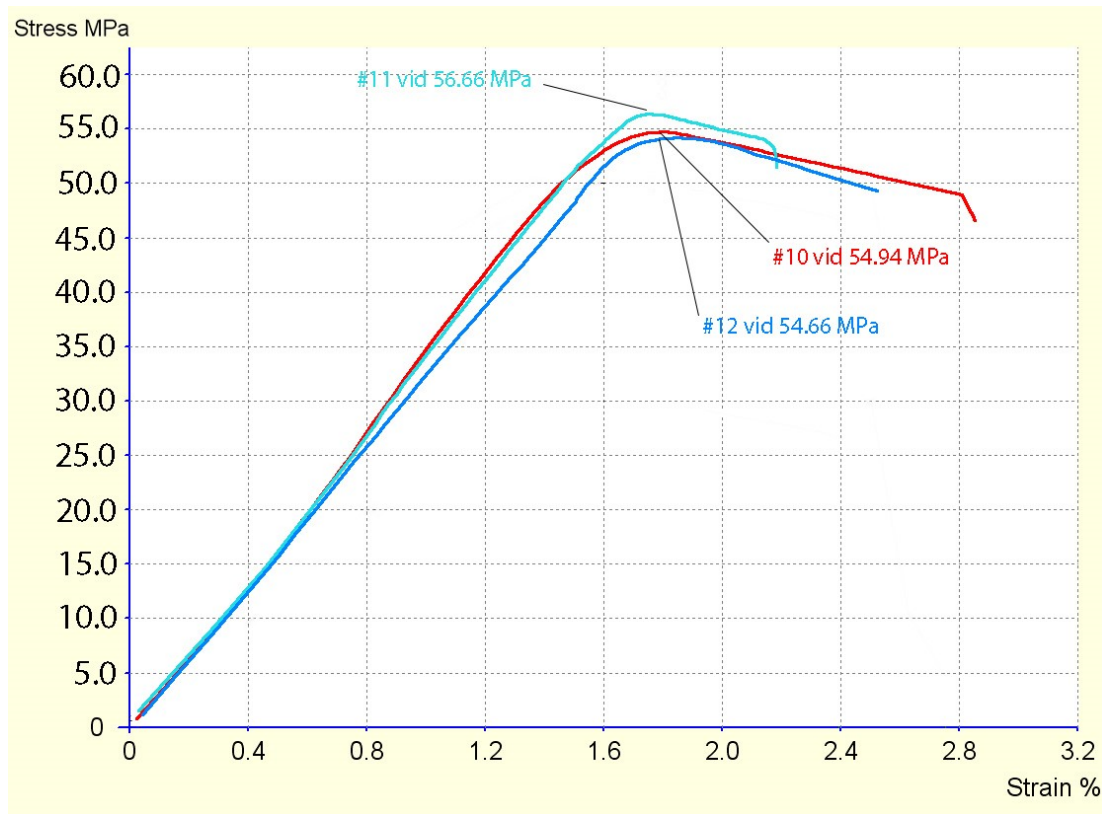


Fig. 8.17. Graph of tensile test results - vacuum-printed ULTEM 1010 specimens

The tensile fracturing mode for all ASA specimens took place along the deposited filaments. A similar way of fracturing is found in the case of ULTEM parts, except for one of the vacuum-printed specimens that fractured transversely, a sign that the deposited filaments of material had enhanced adhesion.

8.4 THERMAL BEHAVIOR OF 3D PRINTED PARTS FROM ULTEM 1010

A discussion must also be made about the heat transfer in the printed parts, to see if the absence of air during the manufacturing process makes a significant difference. Thus, a thermogram by Differential Scanning Calorimetry (DSC) was performed to highlight the thermal transitions in the manufactured parts, namely the glass transition, which is of major importance in determining the temperature range in which the 3D printed parts can be used. Three test specimens were printed for each of the two cases: atmospheric printing and vacuum chamber printing. These were analyzed using a Shimadzu DTA-50 machine (Shimadzu Corp., Kyoto, Japan). The first heating cycle was 20 °C - 280 °C with a temperature rise rate of 5 °C / min, followed by cooling to 30 °C at a rate of 5 °C / min. The second heating cycle was 30 °C - 370 °C at a rate of 10 °C per minute. The analysis was performed in a nitrogen atmosphere at a flow rate of 85 mL / min. The thermal transitions that occurred in the second heating cycle are shown in Figs. 8.19.

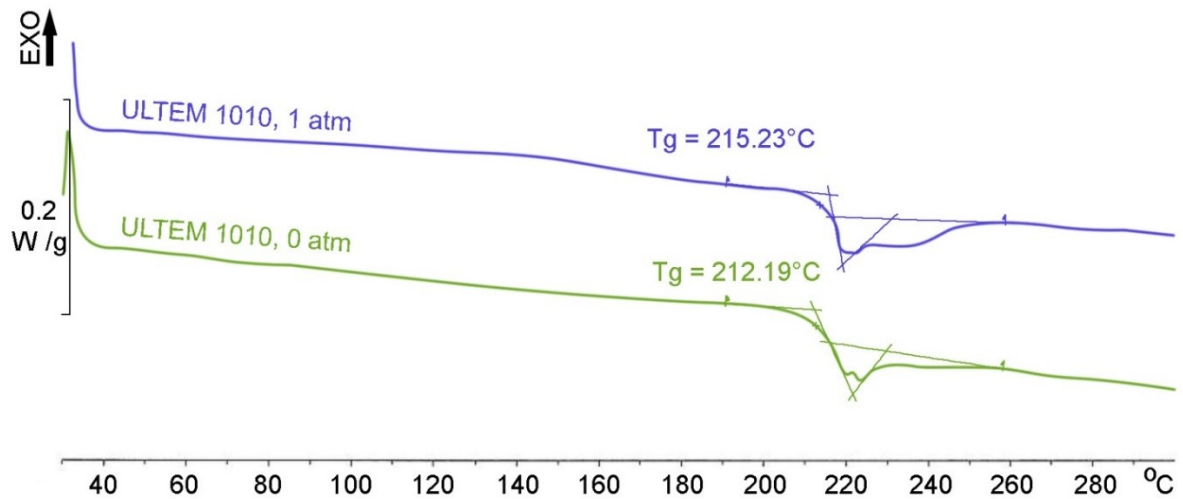


Fig. 8.19. Differential scanning calorimetry thermogram showing the glass transition of the second heating cycle for Ultem 1010 parts

The glass transition for ULTEM 1010 parts printed under atmospheric pressure begins at $T_{g, 1atm} = 215.23$ °C and ends at $T_{pk, 1atm} = 218.02$ °C. These temperatures are in accordance with those found in the data sheet of the material, as well as those found in specialty literature. In the case of parts printed in a vacuum chamber, the glass transition starts at a slightly lower temperature $T_{g, 0atm} = 212.19$ °C and ends at $T_{pk, 0atm} = 220.24$ °C. A possible explanation for this phenomenon would be that the heat transfer in the vacuum printed part is more efficient. Since ULTEM 1010 is a material obtained from amorphous resin, there is no crystallization temperature, the degree of crystallization being 0. Also, the material does not show a melting point, but the fluidity of the material increases once the glass transition temperature is exceeded, reaching a rate flow rate of 17.8 g / 10 min under a load of 6.60 kg, at a temperature of 337 °C

CH. 9 GENERAL CONCLUSIONS, ORIGINAL CONTRIBUTIONS AND FUTURE RESEARCH DIRECTIONS

9.1 GENERAL CONCLUSIONS

During the doctoral study program, research was conducted on the possibility of printing plastics with high melting points in an enclosure with sub-atmospheric pressure, to reduce or eliminate the influence of thermal convection on the properties of printed parts.

The study began with the analysis of existing techniques and applications to date and continued with the investigation of the main constructive types of 3D printers with fused filament fabrication.

In this paper, the process parameters for additive manufacturing by fused filament fabrication were studied. The environmental, dynamic parameters and those related to the filament deposition were treated briefly, with the emphasis on thermal parameters..

In order to visualize and analyze the heat transfer in the part during the manufacturing process, a finite element thermal analysis model was created. With the help of this model certain phenomena could be observed, such as:

- in the case of 3D printers with heated bed, the manufactured part cools starting with the external surfaces, the heated bed having a local influence, restricted to the first layers of deposited material;

- in the case of tall parts, there is a potential to reduce the consumption of electricity used to heat the bed, as maintaining its temperature is no longer necessary to reduce temperature variations (excluding the first layers).

The finite element thermal analysis model was validated through a series of experimental tests, which demonstrate the occurrence of temperature variations inside the manufactured part, by varying thermal parameters, such as the deposition temperature, the type of material (thermal conductivity), the temperature of the heated bed and the temperature of the enclosure in which the material is deposited. Analyzing the results of the experimental measurements, several conclusions can be drawn:

- the heat propagates inside the part in a similar way for all types of material tested;
- the influence of the heated bed is stronger in the case of short parts (small size on the Z axis)
- for materials that require high deposition temperatures, the heated bed is not an effective way to reduce temperature variations.
- both a heated bed and a closed or heated enclosure are valid methods of reducing the temperature variations that occur in the part during the manufacturing process;

In Chapter 6, a new approach to the problem of manufacturing thermoplastic objects with high melting points by fused filament fabrication was discussed, namely the elimination of problems caused by thermal convection by manufacturing in a vacuum chamber. This problem was first analyzed in terms of the behavior of materials in vacuum and at sub-atmospheric pressures. In the second part of the chapter are presented design elements related to the realization of a 3D printer with vacuum enclosure.

For additive manufacturing with ULTEM, PEEK or PPSU material, the extruder nozzle must be maintained at temperatures above 350 ° C. For such an application, the temperature monitoring mode with NTC thermistor is not suitable, it is necessary to change this system with temperature sensors PT100 or with thermocouple type K. These variants can perform accurate measurements in the 200 ... 400 ° C temperature range.

In order to analyze the thermal evolution of the other components of the extruder, a finite element analysis of the temperatures of the extruder components reached during the manufacturing process was used.

The design of the extruder and of the finite element analysis was initially validated by analyzing the performance of the extruder using the parameters recommended by the manufacturer, for ABS type material. Then, thermal analysis was used in case the heating element raises the temperature of the nozzle to 400 °C, the temperature necessary for the extrusion of materials that are being investigated as part of doctoral research activities. The thermal behavior of the extruder during the additive manufacturing process results from the combination of two heat transfer mechanisms. In the first phase, the extrusion nozzle is heated by the ceramic cartridge integrated in the aluminum block. Subsequently, the heat is dissipated from the extruder body by means of forced convection. A finite element analysis has been designed to analyze the thermal performance of the extruder during the extrusion process, depending on the air speed generated by the extruder fan.

Analyzing the results of the thermal analysis with finite elements it can be concluded that, regarding the constructive type and the material from which an extruder capable of processing plastics with high melting temperatures (350 .. 400 ° C) can be made, it is necessary to replace the teflon components from commercial devices with components made of stainless steel..

In the literature there are publications that analyze the surfaces of 3D printed parts in the absence of oxygen. In the experiments presented in these publications, replacing the atmospheric air with inert gas or carbon dioxide, parts with superior surface properties (roughness, better flatness) were produced. In an attempt to verify that these aspects could be repeated under low pressure conditions, test specimens made of ULTEM 1010 material were analyzed using an atomic force microscope. Following this investigation, it was found that the

surfaces of the parts did not undergo significant changes due to the variation of the environment in which they were printed.

Twelve specimens sized according to ASTM D638 type I standard were manufactured in atmospheric conditions and in the vacuum chamber of the 3D printer and subjected to destructive tensile testing.

The dimensional accuracy of the manufactured parts was not significantly influenced by the absence of air in the enclosure, except for the specimens made of ULTEM 1010 material which partially detached from the raft structure due to internal thermal stresses when printed in atmospheric conditions..

The results in figures 8.14-8.17 show that the impact of the absence of air is lower than expected in the case of ASA parts, given the similarity of the polymer to the ABS and the precedents in the literature.

In the case of parts made of ULTEM 1010 polymer, the increases in strength are significant, on average the vacuum-printed specimens being 14% stronger [91].

9.2 ORIGINAL CONTRIBUTIONS

This paper addresses the problem of 3D printing by fused filament fabrication of thermoplastic materials that require high extrusion temperatures. Such temperatures require special printing conditions, as temperature fluctuations resulting from the interaction of the part with the environment lead to defects in parts such as deformations, material accumulations, delamination, etc. After consulting the scientific literature, which describes processes such as printing in a heated room, heating the part during manufacture with infrared lamps or printing in a chamber filled with inert gas, a new solution was developed, namely printing in a vacuum chamber in the absence of air.

In order to understand in detail the heat transfer occurring during the manufacturing process inside a part produced by fused filament deposition, a series of finite element thermal analyses were performed. The method chosen for simulating the thermal behavior of the parts during layer-by-layer manufacturing is of original design and consists in successive thermal analyses that assess the thermal effects produced by each layer of newly added material on the previously deposited material layers. Based on this analysis, temperature graphs were drawn for different sections of the part. The results of finite element thermal analyses were also validated experimentally, using temperature sensors inserted in a rectangular part during the printing process. From the resulting graphs, conclusions were drawn on the development of internal thermal stresses that can lead to delamination defects, as well as on the influence of various parameters such as ambient air temperature or heated bed on the properties of the final part. The gained knowledge was used to develop a study on heat treatments to improve the mechanical strength characteristics of 3D parts made of PETG [92].

Also of original design are the technical solutions developed for building a 3D printer with a sealed vacuum chamber:

- Design of the printer structure and of the vacuum enclosure and their dimensioning by finite elements analysis;
- Design of the drive system for the three axes of the printer, as well as the method of motion transmission through the walls of the vacuum chamber.
- Design of the electrical system and vacuum chamber feedthroughs;
- Building the above-mentioned systems.

Finite element thermal analyses were also done for the thermoplastic material extruder, in order to determine a combination of build materials compatible with the temperatures required for the processing of the investigated printing materials. Finite element analyses were experimentally validated by using temperature sensors attached to two types of extruders.

With the custom-made printer, test specimens were 3D printed and tested destructively and non-destructively. Non-destructive testing includes inspecting the side surfaces of parts with an atomic force microscope to identify potential differences in surface roughness..

Destructive tests were performed to determine the tensile strength of parts printed in the vacuum chamber.

Samples from the manufactured specimens were also subjected to a DSC analysis to analyze the differences produced by the exposure of the materials to low pressure.

9.3 FUTURE RESEARCH

This thesis analysed the feasibility of printing thermoplastic materials with high extrusion temperature in an enclosure where the phenomenon of thermal convection is eliminated by extracting air with a vacuum pump. By designing and building a 3D printer with a vacuum printing chamber it was shown that the printing process is possible. Test specimens with a simple geometry have been successfully printed in this enclosure and have been used for destructive and non-destructive tests. One direction to follow in the future is to establish a profile of process parameters that takes into account the geometry of the printed part in such a way that the heat transfer achieved by thermal conduction through the deposited material allows uniform cooling of the part.

Indeed, from a technical point of view, the solution of using a vacuum chamber is more complex than certain alternatives, such as heating the enclosure or replacing the atmosphere with inert gas, but it also has certain advantages, such as eliminating the need for auxiliary materials (inert gas) and the problems raised by their supply and storage. Also, in the absence of the thermal convection phenomenon, the temperature control in the case of the vacuum enclosure is more precise and does not depend on the dimensions of the side surfaces of the manufactured part, but only on the surface in contact with the printing bed. At the same time, there are applications in which the removal of oxygen prevents the oxidation of the material, such as in the case of filaments impregnated with metal powders.

One approach of interest would be to combine the effect of a vacuum chamber with that of forced convection cooling, made possible by opening the valves of the vacuum chamber and allowing air to enter the enclosure. After cooling, the enclosure can be emptied again. This combination of effects would allow the manufacture of parts with complex geometry such as suspended structures.

BIBLIOGRAPHY

- [1] *Committee F42 on Additive Manufacturing Technologies*. Annual Book of ASTM Standards, **Vol. 10.04**. s.l. : ASTM, 2009.
- [2] *I. Gibson, D. W. Rosen, B. Stucker*. Additive manufacturing technologies – rapid prototyping to direct digital manufacturing 2nd Ed., Springer, 2015;
- [3] *C. W. Hull*. US 4575330 A: Apparatus for production of three-dimensional objects by stereolithography. s.l. : USPTO, 1984.
- [4] *H. E. Menhennet, R. B. Brown*. US 5555176 A: Apparatus and method for making three-dimensional articles using bursts of droplets. s.l. : USPTO, 1994.
- [5] *A. Shkolnik, H. John, A. El-Siblanni*. US 20050248061 A1: Process for the production of a three-dimensional object with an improved separation of hardened material layers from a construction plane. s.l. : USPTO, 2005.
- [6] *C. R. Deckard, J. J. Beaman, J.F. Darrach*. US 5155324 A: Method for selective laser sintering with layerwise cross-scanning. s.l. : USPTO, 1990.
- [7] *Wohlers Associates*. Wohlers Report 2013. s.l. : Wohlers Associates, 2013.
- [8] *Committee F42 on Additive Manufacturing Technologies*. ISO/ASTM52915-16: Standard Specification for Additive Manufacturing File Format (AMF) Version 1.2. s.l. : ASTM, 2014.
- [9] *P. Reeves, D. Mendis*. The Current Status and Impact of 3D Printing Within the Industrial Sector: An Analysis of Six Case Studies. Bournemouth University IPO, Crown, 2015.
- [10] *C. G. Amza, A. Zapciu, D. Popescu*. 3D-Printed shoe last for bespoke shoe manufacturing. 2019, MATEC Web of Conferences 290(1):04001 (**articol indexat BDI in ProQuest**).
- [11] *Materialise*. The Hearing-Aid Industry Will Never be the Same Again. s.l. : Materialise, 2000.
- [12] *D. Popescu, A. Zapciu, C. Tarba, D. Laptioiu*. Fast production of customized three-dimensional-printed hand splints. 2019, Rapid Prototyping Journal, Vol. 26(1), pp. 134–144 (**IF=3.099, Articol în revistă ISI, Q1**).
- [13] *A. Zapciu, C. G. Amza, C. Rontescu, G. Tasca*. 3D-Printed, Non-assembly, Pneumatically Actuated Mechanisms from Thermoplastic Materials. 2018, Materiale Plastice, Vol. 55(4), pp. 517–520 (**articol indexat BDI in SCOPUS**).
- [14] *A. Zapciu, G. Constantin, D. Popescu*. Elastomer overmolding over rigid 3d-printed parts for rapid prototypes. 2018, Proceedings în Manufacturing Systems, Vol. 13(2), pp. 75–80 (**articol indexat BDI in ProQuest, IndexCopernicus**).
- [15] *Wohlers Associates*. Wohlers Report 2014. s.l. : Wohlers Associates, 2014.
- [16] *K. Backman*. Tinkercad has found a new home at Autodesk. s.l. : www.blog.tinkercad.com, 2013.
- [17] *Wohlers Associates*. Wohlers Report 2019. s.l. : Wohlers Associates, 2019.
- [18] *Wohlers Associates*. Wohlers Report 2020. s.l. : Wohlers Associates, 2020 .
- [19] *Research and Markets*. 3D Printing market global outlook and forecast 2020–2025 report, 2020.
- [20] *Sculpteo*. The State of 3D Printing 2020 report, 2020.
- [21] *S. Crump*. US 5121329: Apparatus and method for creating three-dimensional objects. s.l. : USPTO, 1989.
- [22] *B. N. Turner, S. A. Gold*. A review of melt extrusion additive manufacturing processes. 2015, Rapid Prototyping Journal , **Vol. 21**, pp. 250-261.
- [23] *A. Yardimci, T. Hattori, S. I. Guceri*. Thermal Analysis of Fused Deposition. 1997, International Solid Freeform Fabrication Symposium, Austin, TX.
- [24] *Wohlers Associates*. Industry Briefing. s.l. : Wohlers Associates, 2012.
- [25] *N. de Beer, PhD*. - Sierra College CACT. Additive Manufacturing – Turning mind into matter. 2013.
- [26] *R. I. Campbell, D. J. Beer, E. Pei*. Additive Manufacturing în South Africa: building on the foundations. 2011, Rapid Prototyping Journal, **Vol. 17**, pp. 156-162.
- [27] *M. Breittkopf*. A Makerspace takes over a local library. s.l. : Syracuse University – School of Information Studies, 2011.
- [28] *R. Gallant, M. Groenendyk*. 3D printing and scanning at the Dalhousie University Libraries: a pilot project. 2013, Library Hi tech, **Vol. 31**, pp. 31–41.

- [29] *I. V. Antoniac, D. Popescu, A. Zapciu, A. Antoniac, F. Miculescu, H. Moldovan.* Magnesium Filled Poly(lactic Acid) (PLA) Material for Filament Based 3D Printing. 2019, *Materials*, Vol. 12(5)(719) **(IF=3.057, Articol în revistă ISI, Q2).**
- [30] *C. G. Amza, A. Zapciu, D. Popescu.* Paste Extruder—Hardware Add-On for Desktop 3D Printers. 2017, *Technologies*, Vol. 5, pp 50–63 **(articol indexat BDI in ProQuest).**
- [31] *C. G. Amza, A. Zapciu, D. Popescu.* Dispozitiv tip extruder de materiale maleabile, pentru imprimantă 3D. **Brevet RO 132300B1**, 2019.
- [32] *C. G. Amza, A. Zapciu, A. Eythorsdottir, A. Bjornsdottir, J. Borg.* Mechanical properties of 3D printed composites with ABS/ASA substrate and glass fiber inserts. Ianuarie 2019 MATEC Web of Conferences 290(4):04002 **(articol indexat BDI in ProQuest).**
- [33] *C. G. Amza, A. Zapciu, A. Eythorsdottir, A. Bjornsdottir, J. Borg.* Embedding Ultra-High-Molecular-Weight Polyethylene Fibers în 3D-Printed Poly(lactic Acid) (PLA) Parts. 2019, *Polymers*, Vol. 11:1125 **(IF=3.426, Articol în revistă ISI, Q1).**
- [34] *A. Wheeler.* Crowds Roar as 3D Printing Filament goes Electric. s.l. : www.3dprintingindustry.com, 2015.
- [35] *B. Krassenstein.* Graphene 3D Lab Introduces New Graphene 3D Printing Material. s.l. : www.3dprint.com, 2015.
- [36] *A. Zapciu, G. Constantin.* Additive manufacturing integration of thermoplastic conductive materials în intelligent robotic end effector systems. 2016, *Proceedings în Manufacturing Systems*, Vol. 11, pp. 201–206 **(articol indexat BDI in ProQuest, IndexCopernicus).**
- [37] *A. Zapciu, G. Constantin, D. Popescu.* Adaptive robotic end-effector with embedded 3D-printed sensing Circuits. Ianuarie 2017, MATEC Web of Conferences, 121:08008 **(articol indexat BDI in ProQuest).**
- [38] *E. Krassenstein.* Rubber3DPrinting's Conductive TPU Filament Has Incredible Potential for Robotics, Prosthetics and more. s.l. : www.3dprint.com, 2014.
- [39] *W. Wang, T. Y. Wang, Z. Yangy, L. Liu, X. Tong.* Cost-effective Printing of 3D Objects with Skin-Frame Structures. 2013 *ACM Transactions on Graphics*, Article No.: 177.
- [40] *J. Vanek, J. A. G. Galicia, B. Benes.* Clever Support: Efficient Support Structure Generation. Eurographics Symposium on Geometry Processing, 2014.
- [41] *J. Kranz, D. Herzog, C. Emmelmann.* Laser additive manufacturing of lightweight structures în TiAl6V4 – a design for manufacturing approach. Munich : s.n., 2014. iLAS.
- [42] *I. Gibson, D. W. Rosen, B. Stucker.* Additive manufacturing technologies - rapid prototyping to direct digital manufacturing 2nd Ed. s.l. : Springer, 2015, pp 375–397.
- [43] *D. Gunther, B. Heymel, J. F. Günther, I. Ederer.* Continuous 3D-printing for additive manufacturing., 2014, *Rapid Prototyping Journal*, Vol. 20, pp. 320–327.
- [44] *K. Goldberg, M. Golberg.* XY Interpolation Algorithms..May/June, 1983, *Robotics Age*.
- [45] *S. Graves, J. C. Rocholl* (Rostock) *Style Delta Robot Kinematics*. s.l. : Published online, 2013.
- [46] *D. Popescu.* Modelare tridimensională și fabricație aditivă. ISBN 978-606-562-514-3 : Editura Aius.
- [47] *MIT Center for Bits and Atoms.* Fab Central. [Online] [Cited: 1 20, 2017.] academy.cba.mit.edu/classes/computer_design/index.html.
- [48] *D. Popescu, A. Zapciu, C. G. Amza, B. Florin, R. Marinescu.* FDM process parameters influence over the mechanical properties of polymer specimens: A review. 2018, *Polymer Testing*, Vol. 69 **(IF=3.275, Articol în revistă ISI, Q1).**
- [49] *S. N. Halidi, A. Mohd, J. Abdullah.* Moisture and Humidity Effects on the ABS Used în Fused Deposition Modeling Machine. Octombrie 2012, *Advanced Materials Research*, Vol. 576, pp. 641–644.
- [50] *A. Malpot, F. Touchard, S. Bergamo.* Effect of relative humidity on mechanical properties of a woven thermoplastic composite for automotive application. s.l. : Elsevier, Mai 2016, *Materials & Design*, Vol. 98, pp. 12–19.
- [51] *I. Claveria, D. Elduquea, J. Santolaria, C. Pina, C. Javierre, A. Fernandez.* The influence of environmental conditions on the dimensional stability of components injected with PA6 and PA66. [ed.] Elsevier. Aprilie 2016, *Polymer Testing*, Vol. 50, pp. 15–25.
- [52] *K.G. Jaya Christiyan, U. Chandrasekhar, K. Venkateswarlu.* A study on the influence of process parameters on the Mechanical Properties of 3D printed ABS composite. s.l. : IOP Publishing , 2016. IOP Conf. Series: Materials Science and Engineering 114 .

- [53] *J. W. Zhang, A. H. Peng.* Process-parameter optimization for used deposition modeling based on Taguchi method. 2012, *Advanced Materials Research*, **Vol. 538**, pp. 444–447.
- [54] *G.P. Kumar, S.P Regalla.* Optimization of support material and build time in fused deposition modeling (FDM). 2012, *Applied Mechanics and Materials*, **Vol. 110**, pp. 2245–2251.
- [55] *S. H. Ahn, M. Montero, D. Odell.* Anisotropic material properties of fused deposition modeling ABS. 4, 2002, *Rapid Prototyping Journal*, **Vol. 8**, pp. 248–257.
- [56] *O. Lužanin, D. Movrin, M. Plančak.* Effect of layer thickness, deposition angle, and infill on maximum flexural force in FDM-built specimens. 2014, *Journal for Technology of Plasticity* **Vol. 39**.
- [57] *K. Thrimurthulu, P.M. Pandey, N.V. Reddy.* Optimum part deposition orientation in fused deposition modeling. s.l.: Elsevier, 2004, *International Journal of Machine Tools and Manufacture*, **Vol. 44**, pp. 585–594.
- [58] *M. Domingo-Espin, S. Borrós, N. Agulló, A. García-Granada, G. Reyes.* Influence of Building Parameters on the Dynamic Mechanical Properties of Polycarbonate Fused Deposition Modeling Parts. 2014, *3D Printing Additive Manufacturing*, **vol 1**, pp. 70–77.
- [59] *K. Shwetha, H. N. Narasimha Murthy, K. V. S. Rajeswara Rao, N. S. Narahari, R. Agarwal, R. Singh.* Parametric study of Fused Deposition Modelling by Design of Experiments. 2017, *International Journal Of Advancement In Engineering Technology, Management and Applied Science*, pp. 202–212.
- [60] *A. Bagsik, V. Schöppner.* Mechanical properties of fused deposition modeling parts manufactured with ULTEM*9085. 2011. ANTEC.
- [61] *H. Brooks, A. E. W. Rennie, T. N. Abram, J. MCGovern, F. Caron.* Variable Fused Deposition Modelling – Concept Design and Tool Path Generation. Leiria, Portugal : s.n., 2011. *Innovative Developments in Virtual and Physical Prototyping: Proceedings of the 5th International Conference on Advanced Research in Virtual and Rapid Prototyping*. pp. 511–517.
- [62] *T.Nancharaiyah, D. R. Raju, V. Raju.* An experimental investigation on surface quality and dimensional accuracy of FDM components. 2010, *International Journal of Emerging Technologies* 1(2), pp. 106–111.
- [63] *B. Huang, S. H. Masood, M. Nikzad, P. R. Venugopal, A. Arivazhagan.* Dynamic Mechanical Properties of Fused Deposition Modelling Processed Polyphenylsulfone Material. 2015, *American Journal of Engineering and Applied Sciences* .
- [64] *O. Diegel, B. Huang, I. Gibson.* Getting rid of the wires: Curved Layer Fused Deposition Modeling in Conductive Polymer Additive Manufacturing. 2011, *Key Engineering Materials*, **Vols. 467–469**, pp. 662–667.
- [65] *N. A. Sukindar et. al.* Analysis on the impact process parameters on tensile strength using 3D Printer Repetier-Host software. 2017, *ARNP Journal of Engineering and Applied Sciences*
- [66] *C. Page, M. Park, S. Kreuzer, F. Ansari, D. Eason, E. Hamed, H. Watson.* Optimizing 3D Printed Components: A Methodological Approach to Assessing Print Parameters on Tensile Properties. Anaheim, USA : s.n., 2017. *SPE ANTE*. pp. 82–88.
- [67] *N. A. Sukindar et. al.* Analyzing the effect of nozzle diameter in fused deposition modeling for extruding polylactic acid using open source 3D Printing. 2016, *Jurnal Teknologi*.
- [68] *R. Jerez-Mesa, J. A. Travieso-Rodriguez, X. Corbella, R. Busqué, G. Gomez-Gras.* Finite element analysis of the thermal behavior of a RepRap 3D printer liquefier. 2016, *Mechatronics*, **Vol. 36**, pp. 119–126.
- [69] *A. Bellini, S. Guceri, M. Bertoldi.* Liquefier Dynamics in Fused Deposition. 2, 2004, *Journal of Manufacturing Science and Engineering*, **Vol. 126**, pp. 237–246.
- [70] *University of Cairo.* MPE 635: Electronics Cooling. [Online] [Cited: 12 21, 2016.] <http://pathways.cu.edu.eg/ec/>.
- [71] *Nickel, A. H, Barnett, D. M. and Prinz, F. B.* Thermal Stresses and Deposition Patterns in Layered Manufacturing. 2001, *Materials Science and Engineering: A*, **Vol. 317**, Issues 1–2, pp. 59–64.
- [72] *R. K. Sahu, S. Mahapatra, A.K. Sood,* A study on dimensional accuracy of fused deposition modeling (FDM) processed parts using fuzzy logic., 2013, *Journal for Manufacturing Science and Production*, **Vol. 13**, pp. 183–197.
- [73] *Y. Zhang, K. Chou.* A parametric study of part distortions in fused deposition modelling using three-dimensional finite element analysis. 2008. *IMechE* **Vol. 222** Part B: *J. Engineering Manufacture*. pp. 959–967.

- [74] *M. Domingo-Espin, J. M. Puigoriol-Forcada, A-A. Garcia-Granada, J. Llumà, S. Borros, G. Reyes.* Mechanical property characterization and simulation of fused deposition modeling Polycarbonate parts. 2015, *Materials & Design*, **Vol 83**, pp. 670–677.
- [75] *C. Ziemian, M. Sharma, S. Ziemian.* Anisotropic Mechanical Properties of ABS Parts Fabricated by Fused Deposition Modeling. [book auth.] Murat Gokcek. *Mechanical Engineering*. s.l. : InTech, 2012, Ch. 7.
- [76] *M. Montero, S. Roundy, D. Odell.* Material characterization of fused deposition modeling ABS by designed experiments. Cincinnati, OH, SUA : s.n., 2001. *Proceedings of Rapid Prototyping and Manufacturing Conference*.
- [77] *A. Yardimci, T. Hattori, S. Guceri.* Thermal Analysis of Fused Deposition. 1997, *Rapid Prototyping Journal*, pp. 689–698.
- [78] *I. Gestring, D. Mewes.* Degassing of molten polymers. 16, August 2002, *Chemical Engineering Science*, **Vol. 57**, pp. 3415–3426.
- [79] *E.W. Roberts, M.J. Todd.* Space and vacuum tribology. 1, February 1990, *Wear*, **Vol. 136**, pp. 157–167.
- [80] *A. Merstallinger, E.S. Semerad, B.D. Dunn.* Cold Welding due to Fretting under High Vacuum, Helium and in Air. ESTEC, Noordwijk, ESA : s.n., 1997. 7th European Space Mechanisms and Tribology Symposium. p. 223.
- [81] *A. Merstallinger, E.S. Semerad, B.D. Dunn.* Influence of Coatings and Alloying on cold welding due to impact and fretting. San Sebastián, Spain : s.n., 2003. *Proceedings of the 10th European Space Mechanisms and Tribology Symposium*.
- [82] *L.D. Jaffe, J. B. Rittenhouse.* Behavior of Materials in Space Environments, Report No. 32–150 CIO, JPL;. JPL. s.l. : Report No. 32–150 CIO.
- [83] *H. E. Frankel.* Effect of vacuum on materials. 6th ESRO Summer School lecture.
- [84] *Baza de date pentru rate de degazare, „Outgassing Data for Selecting Spacecraft Materials Online”.* [Online] 03 25, 2018. outgassing.nasa.gov.
- [85] *F. Lederle, F.Meyer, G-P. Brunotte, C. Kaldun, E. G. Hübner.* Improved mechanical properties of 3D-printed parts by fused deposition modeling processed under the exclusion of oxygen . 2016, *Prog Addit Manuf*, **Vol. 1**, pp. 3–7. DOI 10.1007/s40964-016-0010-y.
- [86] *Pololu.* Driver motor pas cu pas Allegro A4988. [Online] [Cited: 07 18, 2019.]
- [87] *Marlin.* Marlin Firmware. [Online] [Cited: 07 18, 2019.] <http://marlinfw.org/>.
- [88] *ASTM International.* ASTM D638 – 14 Standard Test Method for Tensile Properties of Plastics. 2014.
- [89] *SNH Mazlan, et al.* Influence of inert gas assisted 3D printing machine on the surface roughness and strength of printed components. 2018. *Mechanical Engineering Research Day, At Malaysia*.
- [90] *wikipedia.org.* Microscopie de forță atomică. [Online] [Cited: 07 19, 2019.] Licență de liberă distribuție CC BY-SA 4.0.
- [91] *A. Zapciu, G. Constantin,* Mechanical properties of thermoplastic polymers 3d printed in a low vacuum environment, *Proceedings in Manufacturing Systems*, **Vol. 15**, Issue 4, 2020, pp. 185-190 **(articol indexat BDI in ProQuest, IndexCopernicus).**
- [92] *C. G. Amza, A. Zapciu, G. Constantin, F. Baci, M. I. Vasile.* Enhancing Mechanical Properties of Polymer 3D Printed Parts. *Polymers* 2021, **Vol. 13**, 562. <https://doi.org/10.3390/polym13040562>, Published: 13 Feb 2021, WOS:000624260800001 **(IF=3.426, Articol în revistă ISI, Q1).**